# THE GIANT PLANET FACILITY

Warren Winovich and William C. A. Carlson

Ames Research Center
National Aeronautics and Space Administration
Moffett Field, California 94035

25th ISA Symposium

Anaheim, 1979

# THE GIANT PLANET FACILITY

Warren Winovich and William C. A. Carlson
Ames Research Center
National Aeronautics and Space Administration
Moffett Field, California 94035

ABSTRACT

The Giant Planet Facility is an electric-arc-jet facility capable of simulating the heating environment for entry into the atmosphere of Jupiter. The facility produces a testing regime hitherto unavailable in arc-jet plasma facilities. It is rated at 100 MW and operates with a hydrogen-helium gas mixture to produce a stagnation-flow region with simultaneous high radiative and convective heating. The significance of this flow regime is that it permits the measurement of the ablation performance of materials under conditions of massive boundary-layer blowing, thus making it possible to assess the coupling that exists between radiative and convective heating. Such basic measurements are vital to the design of the heat shield for a probe entering the atmosphere of Jupiter. Entry into Jupiter's atmosphere occurs at a relative speed of 48 km/sec, and the resulting severe heating environment is dominated by gas-cap radiation from the shock-heated flow. Preliminary tests have been made in the Giant Planet Facility to establish the degree of simulation that can be obtained and to verify facility design techniques. Total heat-transfer rates of 26 $kW/cm^2$—including a radiative component of 8 $kW/cm^2$—have been measured on blunt test bodies 4 cm in diameter. These high heating rates attained in the facility closely match the rates predicted over most of the heat shield. The extremely high radiative heating at the stagnation point of the heat shield will be within a factor of 2 to 4 of projected facility capabilities. This paper summarizes the design concepts for specifying the arc heater and nozzle system, the hardware development, the calorimetry design for facility calibration and testing, and the operational performance limits of the facility.

## INTRODUCTION

During the hypersonic entry into Jupiter's atmosphere, a planetary probe will be subjected to a thermal environment far more severe than that encountered by any previous entry vehicle. The design of the heat shield and the shield's response to such severe heating are critical technical problems. Up to the present time, entry speeds into Earth and planetary atmospheres have been below 12 km/sec (e.g., Apollo at 11 km/sec and Pioneer Venus probes at 12 km/sec). For such entries, the aerodynamic heating has been essentially a convective process. A planetary probe that enters Jupiter's atmosphere will have an initial velocity of 48 km/sec. For such an entry speed, the gas entering the shock-wave layer undergoes such large temperature and pressure increases that it becomes a powerful source of radiative heating; thus, radiation becomes the dominant mechanism for heat transfer to the body. Early analyses (1,2) predicted a "radiation barrier" that would prohibit utilization of entry probes at hypersonic speeds in the meteor range (30-70 km/sec) without the development of special techniques. Such special methods for the design of thermal protection systems for this application were suggested by Allen, Seiff, and Winovich (3) in which blunted cones were shown to be optimum shapes. More recently, detailed analyses have extended their concept by refining the heat-transfer and ablation theories (4,6). Even for so-called optimum heat-shield designs, trajectory analyses indicate that total stagnation heating rates of the order of 60 $kW/cm^2$ will occur (7,8). These heating rates are so high that the heat shield, even with high-performance graphitic materials, will constitute a major portion of the entry mass (e.g., 50%). Consequently, the performance of the heat shield assumes a critical role in determining the success of the mission. Major shortcomings exist in the technology, for heat-shield design for this application: (1) no experimental data exist regarding the absorption effects of the ablation vapors in coupled convective and radiative heating environments with massive boundary-layer blowing; and (2) the analytical models of the ablative performance of carbonaceous materials under conditions of very high radiation are uncertain. This lack of information and the uncertainty in material response in the coupled heating environment established the need for an experimental facility to simulate the Jupiter heating case.

The Giant Planet Facility was designed specifically to simulate the heating enviroment for a Jovian planetary probe. The design precept is based on simulating the expected entry environment to the fullest extent possible by an arc-jet facility in which an optimum test body shape specification ensures that maximum radiative heating rates will be attained. Accordingly, this paper reviews the simulation requirements established by the entry trajectory and a specific probe design. The development of the Giant Planet Facility for simulating the thermal requirements is described with special emphasis on the arc-heater design features necessary to obtain the high energy flow. Special calorimetry techniques are presented which had to be devised since the facility that evolved represents about an order of magnitude increase in heating capability over previous simulation facilities. The performance level of the facility, established by special instrumentation and by the calorimetry techniques, is compared. Additionally, results from computer studies which model the arc-heater operation are compared with calibration measurements that establish the high performance level attained in this new facility.

SYMBOLS

| | |
|---|---|
| $a$ | surface absorption coefficient |
| $a(\lambda)$ | spectral surface absorption coefficient |
| $A$ | cross-section area |
| $B(\lambda,T)$ | Planck function, Equation (17b) |
| BR | blockage ratio |
| $c$ | specific heat |
| $C$ | speed of light |
| $C_D$ | drag coefficient |
| $C_H$ | Stanton number |
| $d$ | test body diameter |
| $D$ | nozzle diameter |
| $e$ | thermocouple voltage |
| $E$ | voltage potential |
| $\dot{E}$ | voltage gradient |
| $F$ | ratio of total to convective heating |
| $G$ | ratio of enthalpy potential to total value |
| $h$ | enthalpy |
| $H$ | Planck constant |
| $I$ | current |
| $j$ | current density |
| $k$ | Boltzmann constant |
| $L$ | length |
| $m$ | mass |
| $\dot{m}$ | mass flow rate |
| $M$ | Mach number |
| $n$ | gas interaction constant, Equation (4-B) |
| $N_o$ | Avogadro number |
| $N_r$ | Reynolds number |
| $p$ | pressure |
| $P$ | power |
| Pr | Prandtl number |
| $\dot{q}$ | heat-transfer rate |
| $r$ | radius |
| $R$ | radius of curvature |
| Rg | gas constant |
| $S$ | distance along surface |
| $t$ | thickness |
| $T$ | temperature |
| $V$ | velocity |
| $z$ | altitude |
| $\alpha$ | entry angle |
| $\gamma$ | isentropic coefficient |
| $\delta$ | shock standoff distance |
| $\eta$ | efficiency |
| $\kappa$ | mass absorption coefficient |
| $\lambda$ | wavelength |
| $\mu$ | viscosity |
| $\xi$ | collision diameter |
| $\rho$ | density |
| $\sigma$ | Stefan-Boltzmann constant |
| $\tau$ | time |
| $\phi(h_t)$ | implicit efficiency function, Fig. 16 |

Subscripts and Superscripts

| | |
|---|---|
| a | ambient |
| abs | absorbed |
| b | test body |
| c | convective |
| e | entry |
| m | melt point |
| N | hemispherical nose |
| o | centerline |
| oc | open circuit |
| r | radiative |
| R | rated |
| t | total state |
| t1 | total state ahead of normal shock |
| t2 | total state behind normal shock |
| TC | thermocouple |
| w | wall |
| 1 | ahead of normal shock |
| 2 | behind normal shock |
| * | nozzle throat value |
| – | mass-average value |

SIMULATION REQUIREMENTS

The entry conditions for a planetary probe designed to study the atmosphere of Jupiter were determined by mission analysis studies (9). The mission sequences are shown in Figure 1. The planetary probe, contained within the heat shield, enters the atmosphere at an altitude of 450 km at an entry angle of -7.50° and at an inertial velocity of 60 km/sec. Because of the high rotational speed of Jupiter (12 km/sec), the relative entry angle will be -9.35° and the relative velocity will be 48 km/sec. Preliminary studies also indicate that a spherically blunted, 45° half-angle conical shape should be adopted for the entry configuration. The entry configuration will have a ballistic coefficient ($m/C_DA$) of 173 kg/m$^2$ to account for an instrumented probe and the conical heat shield. The entry trajectory for such a planetary probe is shown in Figure 2. The atmospheric model specified for Jupiter and the ballistic parameters of the probe will influence the trajectory analysis. For the nominal atmospheric model (10,11) and the assumed ballistic coefficient, the entry probe decelerates rapidly after reaching an altitude of about 200 km. As the probe decelerates, the heat shield undergoes conditions of maximum convection heating, radiation heating, and impact pressure within narrow altitude limits of 125-150 km. These conditions have an important bearing on the requirements for simulating the entry in a test facility.

### Arc-Jet Simulation

The important parameters for arc-jet simulation can be obtained once the trajectory has been established. These parameters, the total enthalpy and the impact pressure, are shown superimposed on the entry trajectory shown in Figure 2. The total enthalpy is determined from the hpyersonic approximation of the energy equation; that is,

$$h_t = V^2/2 \tag{1}$$

The impact pressure is obtained directly from the trajectory analysis as well. The upper atmosphere of Jupiter (45-450 km) can be taken as an isothermal layer for which an exponential density-altitude relation prevails (12). By combining this relation with the hypersonic approximation of the momentum equation, the impact pressure on the entry vehicle can be expressed in parametric form with the altitude and the velocity:

$$z = 31 \ln(V^2/p_{t2}) \tag{2}$$

The arc-jet parameters, enthalpy and impact pressure, which occur near the peak heating zone on the trajectory, establish the simulation conditions for the arc-jet flow. As noted previously, the heating maxima occur nearly simultaneously; consequently the enthalpy level can be selected near the value corresponding to peak radiative heating. The impact pressure given by the parametric relation remains essentially constant at 5 atm throughout the heating period. For the assumed entry case, then, the arc-jet simulated flow conditions are taken from Figure 2 as: (1) enthalpy = 600 MJ/kg; and (2) impact pressure = 5 atm. For a hydrogen-helium gas mixture, these simulation requirements correspond to a stagnation temperature of 15,000 K. In addition to providing a simulated arc-jet flow, the facility must be capable of providing for the closest possible simulation of the expected levels of heat transfer to the entry probe. These heat-transfer rates are determined from the trajectory analysis and from the specific probe geometry that has been adopted.

### Entry Stagnation-Point Heating

The aerodynamic and probe packaging constraints considered in the mission analysis studies have determined the spherical nose bluntness ratio to be 50% and the base diameter of the cone to be 1.245 m. This fixes the hemispherical nose radius as 0.31 m. Accordingly, stagnation-point heat-transfer rates are computed from theories for flow fields about hemispheres. The radiative heating from the shock-wave layer includes nonadiabatic and absorption effects predicted for the stagnation flow (13-15). The convective heating to the surface has been computed from the gradients obtained from a detailed solution of the high-temperature laminar boundary-layer flow. It should be recognized that the calculated rates can change significantly as the atmospheric model changes and as refinements are introduced into the complex heat-transfer theories. The stagnation-point heat-transfer rates for the entry probe have been computed for the specified trajectory and are shown in Figure 3. The heating at the nose is dominated by the radiative component, which has a peak value of 59 kW/cm$^2$ and occurs over a pulse time of 12 sec. The convective heating has a peak value of 18 kW/cm$^2$ and a pulse time of 21 sec. Impact pressure increases only slightly during the heating pulses and is between 5 and 6 atm at peak conditions. The calculated heating rates represent cold-wall values and do not include effects of boundary layer blowing due to ablation of the heat shield material. Convective heating will be blocked virtually completely by the ablation process; however, the corresponding process for the radiative component is not well understood. No experimental measurements are available from simulated heating tests to verify the computational methods for predicting material response to such coupled convective and radiative flows.

The problem of attaining the severe simulated heating rates corresponding to a Jupiter probe entry is illustrated by the technology requirements for ablation testing facilities shown in Figure 4. For a specified spacecraft mission, the entry heating requirements are shown in terms of the convective and radiative heat-transfer rates encountered. The development and testing of the thermal protection system for each application has required that simulation-facility development keep pace with the technology demand. For many applications, the aerodynamic heating is almost entirely a convective heating process. High-pressure arc-jet facilities have been developed that simulate convective heating rates on large test bodies (e.g., bodies 4 cm in diameter) up to levels of 1-10 kW/cm$^2$ (16). As the entry velocity of the spacecraft increases, the radiative component increases as well. The high-speed entry that occurs for missions to Venus, for example, results in radiative heating comparable to the convective heating. Radiant heat sources used in combination with arc-heated nozzle flows were developed to meet this application. The simulation of absorption effects in the boundary layer can be achieved at moderate radiation levels by employing spectral filtering to approximate the gas-cap radiation. Laser radiation can attain high heat-transfer rates; however, important absorption effects can not be evaluated. The simulation requirements for the Jupiter probe entry present the most stringent demand for a simulation facility. The requirement for simultaneous high convective and radiative heat-transfer rates with good spectral simulation led to the development of the high-temperature, high-power, constricted-arc-jet Giant Planet Facility.

## FACILITY DESCRIPTION

The test facility is shown schematically in Figure 5. It consists of a 6-cm constricted-arc heater coupled directly to a low-Mach-number, supersonic nozzle (M = 1.67). The nozzle discharges as a free jet into a walk-in test chamber that is 2.6 m on a side. The test models are mounted on four quick-acting sting supports. As many as four models can be inserted into the test stream for any set operating condition. Precise insertion time and exposure duration are controlled by a programmable timer that is an ancillary part of an automatic gas-flow control system. The test chamber exhausts into a 5-stage steam ejector system during the starting mode and is vented to atmosphere during the high-pressure running mode. During the starting sequence at low pressures, pure argon flows through the system to initiate the arc discharge (argon has the lowest value of spark-breakdown voltage of any gas). After the discharge is established, the system operates on pure nitrogen during the second-stage pumping mode in which the steam ejector system is isolated and the system pressure is increased to the point where the test chamber can be vented to the atmosphere while maintaining supersonic nozzle flow. The pumping mode is accomplished automatically by a programmable digital flow-control system. Finally, for operating at the test condition with the arc current set to the running value, the hydrogen-helium gas mixture is introduced into the arc heater. The flow rate is set at a predetermined value that maintains the pressure in the arc heater at the level established by the nitrogen flow. This is accomplished within about 2 sec by the quick-acting, digital valve.

### Power Supply

Direct current for the arc heater is provided by a power supply consisting of six rectifier modules. Each module consists of a three-phase, full-wave, phase-controlled, silicon-controlled rectifier. The rectifier module contains three parallel strings of silicon-controlled rectifiers arranged to supply a rated current of 2700 A at 4675 V. A schematic view of the power supply is shown in Figure 6a and the voltage-current characteristic is shown in Figure 6b. Each rectifier module is capable of operating over a range from 550 to 4675 V into an arc load. All modules are isolated from ground by insulation rated for 33,000 V. The six rectifier modules can be connected in any compatible series-parallel arrangement by means of remotely operated set-up switchgear. The power supply output configurations are given in Figure 6c. For a duty cycle of 30 min on and 30 min off, the power supply has a rating of 76 MW based on the rated current and voltage. The short-term rating of the power supply is about doubled. For example, for a duty cycle of 15 sec on and 30 min off, with all modules in series, the power supply is rated at 148 MW. The increased rating for short duty cycles can provide the requisite high power for arc-heated simulation facilities. The short-term operation at the higher power levels is consistent with the 10- to 20-sec heating pulses associated with very high speed entry.

### Cooling System

Cooling water for the arc heater is supplied by 10 high-pressure water pumps. The total flow rate is 500 kg/sec at a supply pressure of 45 atm. The cooling system can absorb the entire output from the power supply (148 MW) with a bulk temperature rise of about 70°C. With a supply pressure of 45 atm, the boiling point is elevated to about 250°C. This high-pressure operation allows critical components (i.e., the arc-heater walls) to transfer heat at very high rates without the occurrence of boiling of the bulk flow. In addition to the internal cooling, low-pressure water is supplied for spraying directly into the high-temperature gas stream as it leaves the test chamber. This spray-cooling substantially reduces the heating load to the downstream piping system.

### Operating Sequence with Hydrogen

The use of hydrogen as a component of the test gas requires special precautions to ensure safe system operation. Because the facility uses an electric arc for heating, an ignition source is always present; therefore, the facility is operated such that air is not permitted to come in contact with the working gas in the arc heater, test chamber, or the exhaust system. The arc heater is enclosed within a large duct, and a fan, rated at 12,000 liters/sec (25,000 $ft^3$/min), draws air over the facility and exhausts it outside the building. This air flow, when mixed with the maximum hydrogen leak possible for the facility, results in a mixture considerably below the detonation limit (18%, by volume, Ref. 17). Although the maximum hydrogen leak rate will give a mixture near the combustion limit of 4%, the induced flow velocity in the duct will exceed the flame front velocity and the combustible mixture will be swept outside the building.

In the test chamber, nitrogen is added to the hydrogen-helium test gas during the run to dilute it such that the mixture will not burn when it is exhausted to the atmosphere. After each run, nitrogen is used to purge the system of hydrogen. When the test conditions are such that the nozzle exit pressure is below 1 atm, the test gas is discharged into the vacuum system. The hydrogen-helium test gas is diluted with nitrogen (and steam) so that the mixture will neither detonate nor burn when it finally comes in contact with air. When hydrogen is mixed with water vapor, as it is in the condenser of the steam ejector system, the combustion limit increases; thus, an additional safety margin is provided for flows into the vacuum system (18).

## ARC HEATER DESIGN

The 6-cm constricted-arc heater is the principal component of the Giant Planet Facility. This arc heater is a result of a design philosophy that evolved at Ames Research Center over a number of years. A schematic view of the heater is shown in Figure 7. The arc-heater design is based on the steady-flow, constricted-arc theory developed by Stine and Watson (19,20) and verified experimentally by Shepard, Ketner, and Vorreiter (21). The basic principle underlying this type of arc heater is the operation at very high levels of current density which raises the arc temperature to very high levels. This is accomplished by constricting the arc discharge which causes the voltage gradient to increase along with the temperature. In order to avoid an arc attachment to the confining wall under such high voltage-gradient operation, the constrictor tube must be formed of thin discs such that the arc-column voltage drop along the disc is considerably less than the voltage breakdown level of the discs. This accounts for the characteristic stacked-disc construction of the constricted-arc heater. For the Giant Planet Facility arc heater, the constrictor tube consists of stacked, water-cooled discs packaged in modular form. Each module contains 24 electrically isolated constrictor discs; the discs are 1 cm thick with inside daimeters of 6 cm. A clear plastic material is used as the potting agent for the modules; it permits visual inspection of the discs for indications of inadequate cooling. Eighteen modules, mounted end-to-end, form the constrictor tube. Their total length is 4.32 m. The assembly is sealed for high pressures, possesses good dielectric properties, and is easily handled for assembly.

### Power and Size Determination

In the design of the arc heater, the power rating and the physical size must be considered together since these quantities are closely interrelated. These sizing determinations can be made by applying the facility specifications to the governing arc-heater scaling laws. An approximate analysis is adequate because the facility specifications are not absolutely rigid quantities and the size and power requirements can be relaxed somewhat to ensure that various components operate within physical design constraints. As noted previously, the arc heater is coupled directly to the nozzle to minimize losses, and the sonic flow relation governs the arc-heater flow. Moreover, preliminary considerations indicated that the facility will operate with a low supersonic Mach number and, to first order, the nozzle expansion process can be neglected in the general sizing considerations. With this simplifying assumption, the size of the arc heater is given in terms of the required simulation parameters by the equilibrium sonic flow relation (22):

$$\dot{m}/A^*p_t = 0.016/\sqrt{h_t} \quad (3)$$

The power rating of the arc heater is obtained from the First law relation:

$$\dot{m}(h_t - h_a) = \eta P \quad (4)$$

These equations are combined to yield the power density requirement of the flow in terms of the simulation parameters only:

$$\eta P/A^* = 0.016\ p_t\sqrt{h_t} \quad (5)$$

For sizing calculations of arc-jet facilities that employ the sonic flow relation, the mass-average value of the enthalpy must be used to account for the inherent gradients that exist within the constrictor tube. The mass-average value of the enthalpy can be taken as half of the centerline value. Then, the power density requirement for the facility becomes:

$$\eta P/A^* = 0.016 \times 5\sqrt{600/2} = 1.38\ \mathrm{MW/cm^2}$$

The physical size of the constrictor is selected to satisfy basic facility design constraints. First, the diameter chosen must be compatible with a test-body size requirement since the constrictor serves as the throat of the aerodynamic nozzle and thus determines the size of the test section. Second, the constrictor diameter must be compatible with the power supply rating in order to obtain the power density requirement found above. Finally, the design that results from these sizing considerations must operate at steady-state conditions with an adequate cooling margin for reliability.

The constrictor diameter can be expressed in terms of the test-body size requirement by:

$$D^* = d/\sqrt{(A/A^*)(BR)} \quad (6a)$$

Parametric studies (presented below) show that an optimum value of the area ratio exists. For the specified requirements of the present facility, the optimum value is 1.36—corresponding to a low transonic Mach number flow for the nozzle. Experience in arc-jet operations shows that nozzle blockage ratios up to 3/8 can be employed for stagnation-flow studies. The design criterion, based on test body size as determined by these two ratios, then becomes

$$D^* \approx \sqrt{2}\,d \quad (6b)$$

For obtaining ablation data at reasonable scale in the facility, a requirement for an approximate test-body diameter of 4 to 5 cm was adopted. From the model blockage criterion found above, it follows that the constrictor diameter should be in the range of 5.6 to 7 cm; a constrictor diameter of 6 cm was selected.

The power level of the facility, as determined from the power density requirement for simulation, is specified once the constrictor diameter has been selected. Thus, for a 6-cm constrictor diameter, the input power requirement for the facility (from Equation (5)) is:

$$P = 1.38(\pi/4)6^2/0.4 = 100\ \mathrm{MW}$$

The arc-heater conversion efficiency has been taken as 40% based on prototype development tests and on theoretical computer studies of the design (23). This power level requires that the power supply operate under the short-term rating specification. The length of the constrictor tube was selected on the basis of attaining the requisite power dissipation of 100 MW and on matching the arc-heater load to the voltage-current characteristics of the power supply (Figure 6). This occurs for a constrictor length of 4.32 m.

Accordingly, the 6-cm constricted-arc heater is rated for operation at 100 MW and 5 atm with a current of 7800 A. The flow rate at this condition is 0.13 kg/sec of a 50% hydrogen-50% helium gas mixture (by molar volume). The working gas is injected uniformly along the constrictor via a labyrinth gap between constrictor discs. The 100-MW rating and 6-cm size derived above have been determined by flow simulation and size requirements for the facility. These specifications can only prevail providing that the cooling capacity of the constrictor discs will tolerate the imposed heating. Consequently, the design of the constrictor disc element represents the single most important item in establishing the facility rating and simulation capabilities.

## Constrictor Disc Design

A schematic of the 6-cm constrictor disc is shown in Figure 8. The discs are made of copper and are water-cooled. The unique design feature of the constrictor element is the cusp-shaped water passage. By virtue of this shaped water passage, the constrictor cooling capacity is increased to the degree that its design is compatible with the power rating required for achieving flow and heating simulation conditions. The cusp induces a density gradient within the cooling passage (24). This gradient causes the nucleate boiling bubbles, which occur on the interior surface at high heating rates, to rise from the surface. Without such cusps, a conventional smooth, convex surface has a gradient directed in the opposite directions and the nucleate boiling bubbles formed are stable at the hot-wall surface. When this occurs, the wall cooling capacity decreases drastically to the point where premature (catastrophic) burn-out occurs. Analysis shows that a 12-cusp passage represents an optimum design for obtaining the maximum heat-transfer rate capability of the constrictor discs. This is verified by the heat-transfer rate tests of the constrictor discs shown in Figure 9. A heat source consisting of an arc discharge directed through the disc elements was applied to the conventional and cusp-shaped designs. The applied heating is proportional to the arc current density; the resulting heat-transfer rate to the disc was measured by monitoring flow rate and temperature rise of the cooling water. The designs were subjected to heating to the failure point. The 12-cusp, 2-mm-wall-thickness design exhibits over a twofold increase in heat-transfer rate capability relative to the conventional smooth-wall design. A 3-mm-wall-thickness design also shows an improved performance. These failure-point tests show that the cusp-shaped cooling passage design can survive with heating rates as high as 14 $kW/cm^2$, within 10% of the theoretical limit. The constrictor disc is rated for cooling to 12 $kW/cm^2$ which allows a safety margin to account for manufacturing tolerances, water-side scale deposits, and local flow anomalies.

In addition to high cooling capacity, the other important feature of the constrictor design is a high resistance to voltage breakdown. The constrictor disc thickness and the separating gap must be specified such that the spark breakdown voltage for adjacent discs exceeds the arc-column gradient with a sufficient safety margin. These characteristics for a 1-cm-thick constrictor element with a gap of 0.71 mm are shown in Figure 10. The constrictor breakdown voltage is predicted by the Paschen theory (25) for a wall temperature of 4000 K, which corresponds to the recombination temperature of molecular hydrogen. The arc-column gradient for the hydrogen-helium gas mixture has been measured over a range of operating conditions; the data exhibit a linear relation with pressure. The measured values agree well with data obtained in a shorter, prototype 6-cm arc heater. Also, the measurements substantiate the theoretical prediction of the gradient for the gas mixture. These measurements indicate a design safety margin of a factor of 5 for voltage breakdown at rated pressure (5 atm). The arc has operated up to 4.9 atm without voltage breakdown of the constrictor.

In determining the power rating of the arc heater, the imposed heat-transfer rate to the walls must be compatible with the cooling capacity of the constrictor discs. It can be readily shown that for a given arc heater the heat-transfer rate for maximum current is uniquely determined by the arc-column gradient. Thus,

$$\dot{q}_w = \dot{E}I(1 - \eta)/\pi D \qquad (7)$$

Conservative design procedure suggests that the constrictor walls should dissipate the entire electrical input (i.e., $\eta = 0$). This criterion is consistent with the general observation that the efficiency of constricted-arc heaters decreases as operational design limits are approached. For the 6-cm constricted-arc heater with the present specification (5 atm and 7800 A), the design value of the wall heat-transfer rate becomes:

$$\dot{q}_{w,D} = 30 \times 7.8(1 - 0)/\pi \times 6 \approx 12 \text{ kW/cm}^2$$

This value, compatible with the demonstrated cooling capacity of the constrictor disc design, has been adopted as the design value for the wall heating limit.

The cooling capacity of the constrictors, therefore, is the determining factor in establishing the facility power rating. Moreover, the value of the wall heating found above (Equation (7)) indicates that the constrictor walls are required to operate near theoretical cooling limits to attain the high power level needed to produce the simulated entry heating environment.

### Anode

To accommodate the high current with low contamination levels, the anode assembly is designed with 10 parallel-connected electrodes. Each electrode is capable of operation up to 1000 A. A sketch of the electrode design is presented in Figure 11; details of the design are given in Ref. 26. The anode units are water-cooled copper rings. The arc termination point is driven around the interior surface by a magnetic field generated by a coil located within the electrode (cross-section view, Figure 11). This coil is in series with the anode element; the 1000-A maximum current level is based on a 6-kW heat dissipation limit of the magnetic-drive coil. Contamination of the copper is negligible, due to the high spin rate of the arc foot.

### Cathode

The cathode arrangement is considerably different from that of any other system. For very high enthalpy levels, the arc should terminate in the supersonic nozzle as close to the test section as possible. To reduce radiative and convective losses, this consideration ruled out a conventional cathode location in a plenum ahead of the nozzle. Two cathode arrangements designed to minimize flow losses have been used. In the first design, alternate discs, which form the expanding nozzle, were employed as cathodes. Each active disc was connected in series with a ballast resistor that was tailored to distribute current uniformly between the 15 cathode elements. This configuration proved unreliable at power levels above 50 MW because voltage breakdown occurred across the gaps of adjacent nozzle/cathode elements. At high current levels (over 4500 A), it was observed that the breakdown occurred at regions of minimum magnetic field that were created by the interacting magnetic fields associated with the power leads. Attempts to alter the arc-magnetic field interaction by changes in symmetry of the power leads alleviated the condition only slightly and this configuration was discarded.

In the second configuration, which is also a radical departure from conventional practice, the high temperature properties of the effluent gas are utilized. The high temperature, recirculating gas flow is very conductive. Consequently, electrodes located in the vicinity of the nozzle exit readily conduct current from the arc-jet stream. The high conductivity and the low pressure that exist in the test section ensures that the joule heating will not produce severe, nonuniform local enthalpy gradients. From these considerations, the second cathode configuration shown in Figure 12 evolved. Four graphite cathodes are arranged in a symmetrical pattern 10 cm from the nozzle exit. Each cathode is 4 cm in diameter and 16.5 cm long. The cathode tips are beveled at the Mach angle (31°) in the direction of nozzle flow to avoid interference effects when the nozzle flow departs from the ideally expanded free-jet condition which occurs during the low-pressure starting sequence. The cathode tips are located 15 cm from the centerline of the nozzle and, at full pressure operation, they are well outside the test stream. Although the graphite electrodes wear, carbon-particle contamination of the test stream is minimal. Spectroscopic measurements have been made at the stagnation point of test bodies that verify low contamination levels. Equal current distribution is ensured by placing a ballast resistance of 0.1 ohm in series with each cathode element. This configuration has operated reliably up to power levels of 80 MW.

## NOZZLE/TEST BODY DESIGN

Since radiation is the dominant heating mechanism for the heat shield, it is important to attain maximum values of stagnation temperature, pressure, and shock standoff distance in the test facility. This requires an optimization of the nozzle and test body design. The arc-heater sizing and design features will provide simulated flow conditions at the 100-MW power level. The actual levels of radiative and convective heating attained in the facility, then, depend on the selection of the aerodynamic nozzle and the test model geometry.

### Nozzle Selection

Parametric studies were made to obtain an optimum nozzle and test-body combination. Prior studies (27,28) showed that in order to obtain high radiation heating in arc-jet flows, a blunt body shape is necessary to provide a large radiating volume within the gas cap. Preliminary tests of such blunt shapes further showed that the body size could represent a tunnel blockage ratio as high as 50% at moderate supersonic Mach numbers (e.g., M = 3). The existence of longitudinal gradients introduced by large blockage-ratio models has a negligible effect on the large radial gradients of blunt-body flows within the gas cap and good stagnation flows result. At low supersonic Mach numbers, the blockage ratio must be scaled down to avoid nozzle choking phenomena (29).

The results of such a parametric study are shown in Figure 13. Calculated values of the radiative heat-transfer rate to a flat-faced test body are shown as a function of test-section Mach number. The results are for an optically thin radiating shock layer represented by the relation:

$$\dot{q}_r = 2a\delta(\rho\kappa)\sigma T^4 \tag{8}$$

The formulation of the mass-absorption coefficient $(\rho\kappa)$ is obtained from the detailed stagnation-flow computer solutions of Ref. 30. Shock standoff distance, $\delta$, and the mass-absorption coefficient were calculated as a function of Mach number for the specified total state of 500 MJ/kg and 5 atm. A surface absorptance of unity has been assumed. Details of the analysis are presented in Appendix A.

The analysis shows that radiative heating to a test body in the arc-jet stream decreases as the Mach number of the facility increases. The decrease in the heat-transfer rate is caused by the reduction in stagnation pressure associated with the normal shock pressure recovery that occurs with increasing Mach number. Maximum radiative heating is predicted for a Mach number of 1.60. This maximum occurs because the allowable wind-tunnel blockage factor decreases as Mach number approaches 1. A slight compromise can be made by selecting a slightly higher value for the Mach number to allow for an increase in the physical size of the test body. The arbitrary selection of a much higher Mach number, however, could reduce the level of radiative heating to very low levels.

A similar analysis has been made for the convective heat transfer to the test body; the results are shown in Figure 14. The scaling law used for the convective heating to the test body is adapted from the laminar, stagnation-point theory for hemispheres (31,32):

$$\dot{q}_c = 0.00475\sqrt{p_{t2}/R_N}\,h_t(1-G) \tag{9a}$$

For application to blunt, flat-faced bodies, an effective nose radius must be used to account for the lower velocity gradient. Tests in arc-jet flows have shown that the effective hemispherical nose radius for a flat-faced body is (33):

$$R_N = 3.78\ r_b \tag{9b}$$

The convective heat transfer rate at the stagnation point of the blunt body has been calculated as a function of Mach number for the specified total state of an enthalpy level of 500 MJ/kg and a pressure of 5 atm. Convective heating also decreases as the Mach number increases. In contrast to the radiative component, the convective heat-transfer rate continues to increase as the Mach number approaches unity. Near the optimum Mach number found from the radiative analysis (M = 1.6), the convective heating to the test body will be about 13 kW/cm$^2$ which represents a good simulation to the predicted entry value presented above.

From these considerations of the heating capabilities of the arc-jet system, the Mach number selected for the Giant Planet Facility was 1.67. The nozzle was specified to be a simple conical shape with a half-angle of 0.94° and an exit diameter of 7 cm. The expansion is so slight that contouring of the walls is not warranted to obtain an essentially uniform, parallel nozzle exit flow. The pressure ratio between the total (or arc heater) pressure and the nozzle exit pressure for an ideal free jet is 4.41 from isentropic nozzle flow relations ($\gamma$ = 1.23). Accordingly, for an ideal free-jet nozzle flow into the atmospheric-vented test chamber, the total (arc) pressure must be 4.41 atm—slightly less than the 5-atm-rated operating condition for flow simulation. Operation of the nozzle at pressures much lower than this value will cause the flow to separate within the nozzle and to emerge at a lower Mach number. Operation at higher pressures than the ideal pressure level causes the nozzle flow to be underexpanded, and flow interactions emanating from the free-jet boundary can introduce flow nonuniformities in the test stream. For this reason, the test body is positioned within the uniform flow region of the second test rhombus for both underexpanded and overexpanded free-jet flows.

### Optimum Test-Body Design

Flow blockage criteria specify the test-body size. The blockage ratio criterion adopted for free-jet flows is

$$BR = (d/D)^2 = 0.176\sqrt{M^2-1}, \quad 1 < M < 3 \tag{10}$$

Thus, for a design Mach number of 1.67, and selecting a conservative value for the blockage ratio of about 0.25, the diameter of the test body will be between 3 and 4 cm (for a free-jet diameter of 7 cm). This size satisfies the physical size requirement for ablation testing, and it ensures that no serious problems will occur in starting and maintaining supersonic free-jet flow.

The geometry of the test body is summarized in Figure 15. The basic shape of the test body is a blunt ellipsoid with an aspect ratio of about 0.25. This shape was chosen for two reasons: (1) the shock standoff distance is greatest for blunt bodies, especially for low supersonic speeds, and radiative heating is enhanced; and (2) the blunt ellipsoidal shape is representative of the steady-state shape of an ablated body in arc-jet flows (34). For such blunt ellipsoids (aspect ratio < 0.3), the flow in the stagnation region is influenced strongly by the edge shape—especially at low supersonic speeds (35). This effect causes the shock standoff distance for the blunt ellipsoid shape to be reduced somewhat relative to a flat-faced body; however, it remains virtually constant during ablation tests. Consequently, ablation data from the facility should require no shape-change corrections. The test-body geometry shown in Figure 15 has been adopted for the facility calorimeters, pressure probes, and ablation test models. For machining purposes, the ellipsoid is approximated by specifying the corner radius to be $r_c/r_b = 0.2$; and the front-face surface is specified to have a constant radius of curvature that is 10 times the body radius. The slight curvature of the front surface ensures that the stagnation point remains fixed near the centerline. By contrast, for absolutely flat-faced bodies, a slight angular misalignment causes the stagnation point to shift to the edge of the test body, and the radiative heating near the central test core can be reduced about 25-30%.

## FACILITY PERFORMANCE

The discussion of the performance of the Giant Planet Facility is separated into two main topics: (1) the arc-heater performance and, (2) the heat-transfer rate capabilities attained using special calorimeters developed for the optimum test-body shape previously described. The performance of the arc heater establishes limits for the heating simulation capabilities of the facility. For simulation heating and ablation tests at conditions relevant to the Jupiter probe entry, the facility performance, in terms of attaining high heat-transfer rates (particularly, high radiative heating rates), is important. Both performance characteristics for the Giant Planet Facility are limited by state-of-the-art bounds imposed.

### Arc-Heater Performance

The performance of the arc heater is governed by the energy conversion efficiency. In turn, that efficiency is determined by the heat-transfer losses in the constrictor tube. Both radiative and convective losses exist, and the arc performance characteristics are influenced by the dominance of either convective or radiative heating as the operating power level changes. The efficiency of the arc heater is defined by

$$\eta = \text{output/input} = 1 - \text{losses/input} \qquad (11)$$

The loss mechanisms are convective heating on the inside surface of the constrictor bore, and radiative heat transfer from the confined arc column. With some manipulation, Equation (11) can be written in a simple form that is useful for explaining the performance of constricted arc heaters (26):

$$\eta = 1/[1 + 4(L/D)C_H F] \qquad (12a)$$

where the factor $F$ accounts for radiation losses:

$$F = 1 + \dot{q}_r/\dot{q}_c \qquad (12b)$$

The magnitude of the arc-heater efficiency is determined solely by the three dimensionless parameters: the aspect ratio of the constrictor tube, the Stanton number which governs the convective heating, and the arc-column radiation factor. The aspect ratio of the arc heater is 72 and is fixed by the need for a constrictor length of 4.32 m and the constrictor diameter of 6 cm derived from the power density requirement for flow simulation. The aspect ratio is a constant for specified constrictor geometry. Therefore, the variation in efficiency over the operating range of the facility is controlled by the Stanton number and the radiation factor. These quantities can be readily calculated for the constricted arc using convective heating formulations for fully developed turbulent pipe flow (36) and employing the radiative heating calculation for high-temperature hydrogen-helium mixtures. The radiation from the arc column is calculated on the basis that the effective radiating volume is a cylinder with a diameter that is half the value of the constrictor. The validity of this simple radiating arc-column model has been demonstrated for constricted arcs operating with air. The transport properties for the hydrogen-helium gas mixture have been calculated using mixture rules (37) applied to pure hydrogen and helium. The equation of state was obtained from the computer subroutine of Ref. 23. Details of the calculation are given in Appendix B.

The predicted performance of the 6-cm constricted-arc heater is shown in Figure 16. The efficiency has been calculated for a pressure level of 4 atm. At enthalpy levels below 150 MJ/kg (mass-average value), the efficiency remains relatively constant at a nominal value of 0.45. At low enthalpy levels, the performance is determined virtually by convective losses only. Efficiency decreases only slightly with enthalpy level since the flow in the constrictor tube is turbulent ($N_r$ > 2000) and the Stanton number is inversely proportional to the fifth root of the Reynolds number; consequently, the efficiency remains virtually constant over a wide operating range.

For operation above 150 MJ/kg, the calculated radiation loss from the arc column becomes significant. As enthalpy increases above 150 MJ/kg, the predicted arc efficiency decreases rapidly. Moderate changes in the pressure level have a minor effect on the prediction since compensating effects occur.

Experimental values of the arc-heater efficiency have been obtained by measuring the losses to the cooling water and the electrical power input. The mass-average value of the enthalpy is also experimentally determined by measuring the hydrogen-helium gas mixture flow rate. These values are compared in Figure 16 with the theoretical prediction. The data are for operation at 4 atm, the pressure at which many developmental and facility calibration runs have been made. Good qualitative agreement is obtained between measured and calculated values of arc heater efficiency. In general, the data exhibit the predicted trend in which efficiency decreases as enthalpy increases. However, a few data points in excess of 200 MJ/kg are counter to the trend. The ratio of the centerline temperature to the temperature corresponding to the mass-average enthalpy was determined spectrographically to be 1.35. This ratio determines the enthalpy level at which the efficiency decreases for the case of the theoretical radiating arc-column model.

The sonic flow relation for the hydrogen-helium gas mixture is shown in Figure 17. The mass flux density normalized by the total pressure is plotted as a function of the enthalpy level. For low temperatures, up to the dissociation level of hydrogen (4000 K), the isentropic coefficient of the gas mixture remains constant ($\gamma = 1.50$). As dissociation occurs, the effective isentropic coefficient changes. If chemical equilibrium prevails, the effective isentropic coefficient will be 1.23; if the process is chemically frozen, the value will approach the classical value of 5/3. The measurements of flow rate, arc pressure, electrical power, and efficiency permit arc-heater performance to be determined in terms of the sonic flow formulation. For the range of operation, agreement between theory and experiment indicates that the arc-heater process is in equilibrium. Over the limited test range, the results follow the inverse square-root law that is predicted. The data scatter by about ±10% about the equilibrium flow result (i.e., an isentropic coefficient of 1.23).

Further insight into the performance characteristics of the arc heater is given by the pressure distribution along the arc heater (Figure 18). The pressure distribution exhibits an approximately linear decrease along the constrictor tube length. By adjusting a wall roughness parameter to fix the sonic-point location, predictions from the arc-flow theory (ARCFLO, Ref. 23) agree qualitatively with the experimental results. Near the sonic throat, however, the measured pressure gradient exceeds the computed value by a considerable margin. In the aerodynamic nozzle, which is coupled directly to the arc heater, the measured pressure distribution agrees with the predicted expansion process for isentropic flow with an effective isentropic coefficient of 1.23. This value for the effective isentropic coefficient is consistent with the observation made previously that the arc-heater process is in equilibrium and that the isentropic coefficient can be taken as 1.23. Since there is no plenum chamber ahead of the throat of the nozzle, a virtual stagnation-point location along the constrictor was found by selecting a constrictor disc where the wall static pressure corresponded to the stagnation pressure computed from the sonic nozzle throat pressure. An effective isentropic coefficient of 1.23 was assumed, and the virtual stagnation point was located at the 3.44-m station. This pressure is defined as the virtual total pressure in all performance measurements. The ARCFLO theory was used to substantiate this location. By applying the momentum equation to the results of the nonadiabatic-flow computer solution a reasonable agreement was obtained in which the virtual stagnation-point location was located at the 3.58-m station, just 14 cm downstream.

Once the ARCFLO computer solution was adjusted to obtain the approximate pressure gradient and sonic location, the complete solution could be compared with experimental results. As noted earlier, the voltage gradient was predicted to good accuracy. Consequently, the power level was matched, and the performance predicted by computer solution could be compared with the measured values. This comparison is shown in Figure 19, in which the wall heat-transfer rate distribution is plotted. Over most of the constrictor, the measured heat-transfer rates agree with the computed values within 12%. The measured heating distribution exhibits the opposite trend to the computer solution near the upstream constrictor tube entrance region. This is a critical region of the arc heater in that these locally high heat-transfer rates establish the facility operational limits. The wall heat-transfer rate can also be found from the arc-heater efficiency calculated from Equation (12) (or taken from Figure 16) for the specified power input. This method predicts a constant value of the heat-transfer rate. For the test condition of Figure 19, a value of 3.95 kW/cm$^2$ is obtained; it also agrees reasonably well with the measurements.

The efficiency and heat losses have been well established by the calibration tests summarized previously. In addition, the measurements of the loss mechanisms agree well with theoretical predictions and with equilibrium sonic flow. The facility performance limits based on these losses, then, can be predicted with reasonable certainty.

Facility Performance Envelope

The operating limits of the facility are determined by the arc performance characteristics, cooling limitation, and restraints imposed by inherent material limits. The performance envelope is defined by combining the sonic flow relation (Equation (3)), the First law relation (Equation (4)), and the arc-heater efficiency (Equation (12) or Figure 16). The performance is given in terms of centerline enthalpy which is taken as twice the mass-average value. Spectroscopic measurements indicate that this is the case at the 60-MW power level. The computer simulation of the arc heater shows that this ratio holds over wide power ranges. The result is given in implicit form since the efficiency is not given in closed form. Thus,

$$\begin{aligned} h_{t,0} &= 7812[1/(A^*)^2]P^2\eta^2(1/p_t^2) \\ h_{t,0} &= 2\,\bar{h}_t \\ \eta &= \phi(\bar{h}_t) \end{aligned} \tag{13}$$

For a constant power level, the enthalpy-pressure characteristic for the facility is specified. Results are shown in Figure 20. For any constant power operation, the enthalpy increases as the operating pressure is lowered. For low enthalpy levels, the enthalpy varies inversely with the square of the pressure since the efficiency remains essentially constant. However, for high enthalpy levels (above 400 MJ/kg) where efficiency decreases, the enthalpy level will increase only slightly for low-pressure operation at constant power levels.

The specified upper power rating of the facility is 100 MW. That limit is dictated by the level of constrictor wall heating encountered and the cooling capacity of the constrictor discs. One can show that constrictor wall heating is given in terms of the facility performance parameters as

$$\dot{q}_w = 2\sqrt{2}\,(L/D)\,[(1-\eta)/\eta]\,p_t\sqrt{h_{t,0}} \tag{14}$$

By specifying the constrictor wall heating limit as 12 kW/cm$^2$, the locus of Equation (14) defines the upper facility limit; the limit is shown in Figure 20. Interestingly, the limit coincides with the constant 100-MW power limit for all pressures below 4 atm. The design pressure limit of the arc heater is 10 atm. Between 4 and 10 atm, the facility power level can be in excess of 110 MW without exceeding the predicted cooling limit of 12 kW/cm$^2$, but heating to the test body falls off in this range because the arc temperature is low. The lower limits of the performance envelope are taken as an enthalpy of 100 MJ/kg and a pressure of 1 atm. Data obtained during preliminary calibration tests at power inputs of 20-25 MW and 55-65 MW are in good agreement with the calculated performance levels.

For comparison, two entry trajectories are superimposed over the facility operating envelope. These trajectories define an entry corridor for the mission. The nominal entry at -9.75° is the design value for the planetary probe and the skip-limit entry at about -3.50° defines a minimum condition. The high heating pulse for the entries occurs on either side of the maximum pressure point; it is identified by the shaded area. Maximum heating occurs near 600 MJ/kg for all trajectories. It is apparent that the upper facility power rating of 100 MW imposes a physical limit that prevents a complete matching of the power density of an actual entry by a factor of about 2. As discussed previously, the generation of high heat-transfer rates for entry simulation requires operation near maximum limits of the performance envelope with optimum-shaped test bodies. The measurement of performance in terms of the attainable heat-transfer rates at these maximum facility levels requires special calorimetry methods.

Calorimeter Development

The absorbed total heat-transfer rates for the Giant Planet Facility are so high that steady-state, water-cooled calorimeters cannot be used to make the heating measurements. The transient asymptotic calorimeter which is rapidly swept through the stream (38) was not adaptable because the electromagnetic noise associated with the high-power arc resulted in unacceptable signal-to-noise ratios. Consequently, the thin-skin, transient calorimeter design shown in Figure 21 was adopted. The physical shape is identical to that of the optimum test-body design. Tungsten, formed by the sintered metallurgy process, is used for the calorimeters; the calorimeters are expendable. The tungsten density is about 80% of the pure-metal value. The section thickness was selected from a transient heating analysis to obtain the maximum linear response time for a back-surface temperature measurement (39). The thermocouple for back-side temperature measurement is not attached to the tungsten cap but is mounted in a spring-loaded assembly that forces it against the cap to ensure good thermal contact during any motion of the cap due to thermal stress induced at the high heating rates. To reduce conduction losses, the thermocouple is 0.127 mm in diameter and the thermocouple junction was mounted on a ceramic spherical sector with a very low value of thermal diffusivity. In order to reduce the variation in contact potential between the surfaces, each thermocouple assembly was lap-fitted with the mating tungsten cap. After a short nonlinear transient, the calorimetry equation for the thin section is given by the linear solution:

$$\dot{q} = \rho c t (dT/d\tau) \tag{15}$$

where the density and specific heat of tungsten are taken as constant over the incremental temperature rise. The temperature gradient is obtained directly, using a high-speed recorder, from the linear voltage output of the thermocouple.

A calibration check was performed on each calorimeter using a radiant source that produced a heating rate of about 1 kW/cm$^2$. The source was calibrated using a commercial Gardon-type water-cooled calorimeter. Typically, the calibration at this level agreed within 15% with the thin-skin calorimetry equation using measured property values for tungsten (40). An error analysis shows that uncertainties in material properties at the elevated temperatures associated with the high heating rates are about 15%. Consequently, the calibration at the 1-kW/cm$^2$ level merely reflects this uncertainty, and data are reported with no applied corrections. A light plastic sabot was used to protect the calorimeter during the time required to insert the calorimeter into the stream centerline. High-speed motion pictures show that aerodynamic forces remove the sabot in about 8 msec, which ensures a step-function heating pulse that is implicit in the derivation of the calorimeter equation.

In addition to heat-transfer rate, the impact pressure on a test body was also measured to characterize the nozzle flow and to aide in the correlation and interpretation of the calorimeter data. Impact pressure ratio as a function of the stagnation pressure is shown in Figure 22. The virtual stagnation pressure as measured at the 3.44-m station along the constrictor tube was used as the normalizing pressure for this ratio. For cold flows with the nozzle flowing as a balanced free jet, measured impact ratio equals the theoretical normal shock recovery ratio of 0.84. For the nonadiabatic flow of the hydrogen-helium mixture, the measured impact pressure ratio is about 0.63 over a range of stagnation pressures from 3.5 to 4.6 atm. The low pressure recovery ratios found for hot flow are unexplained. These resulting low values of impact pressure reduce the convective and radiative heat-transfer rates to the test body.

Heat-Transfer Rate Measurements

The heat-transfer rate to the calorimeter is the sum of the convective and absorbed radiative heating:

$$\dot{q}_{abs} = \dot{q}_c + a\dot{q}_r \tag{16}$$

The absorption coefficient of the surface, a, is a spectral weighted mean value. For radiation from the hydrogen-helium gas mixture, the absorptive coefficient can be taken as the Planck mean value:

$$a = \frac{\int_0^\infty a(\lambda)\, B(\lambda,T)\, d\lambda}{\int_0^\infty B(\lambda,T)\, d\lambda} \tag{17a}$$

where

$$B(\lambda,T) = 2\pi H C^2/\lambda^5 (e^{HC/k\lambda T} - 1) \tag{17b}$$

For radiation from a 14000 K source, and for a smooth tungsten surface, the Planck mean absorption coefficient is 0.78.

Absorbed heat-transfer rates for the 4-cm-diameter test body are shown in Figure 23 as a function of power input. All calorimeter measurements are for pressures between 3.5 and 4.6 atm. At a power level of 59 MW, the mean value of the absorbed calorimeter heat-transfer rates is 15 kW/cm$^2$. Also, at 59 MW, a direct measurement of the radiative heating was made using a blackened calorimeter (a = 1.0) with a thin (1 mm) ablating teflon cap which blocked virtually all of the convective heating. A radiative heating rate of 6.0 kW/cm$^2$ was measured by this technique. Assuming the Planck mean absorptivity of 0.78 for the tungsten surface, the convective component can be found to be (15.0 - 0.78 × 6.0) 10.3 kW/cm$^2$.

Using the scaling laws for radiative and convective heat transfer given by Equations (8) and (9), the heat-transfer rates to the 4-cm-diameter test body can be extrapolated to the rated power level of the facility. The scaling proportionalities in simplified form that are valid for extrapolation from the 60-MW to the 100-MW power level are:

$$\dot{q}_r \propto p_t^{0.882} \, h_{t,0}^{5.625} \qquad (18a)$$

$$\dot{q}_c \propto \sqrt{p_t} \, h_{t,0} \qquad (18b)$$

The performance characteristics from the facility envelope (Figure 21) were used to extrapolate the heating capabilities. The results are shown on Figure 23. Extrapolation to the 100-MW power level indicates that convective heating will increase to about 16.5 kW/cm$^2$. Radiative heating increases at a more rapid rate at high power levels, and at the facility power rating of 100 MW, radiative heating to the 4-cm-diameter test body is extrapolated to 17.5 kW/cm$^2$. The total heating for a black surface ($a$ = 1.0) would approach 34 kW/cm$^2$ at the 100-MW rating. With a surface absorptivity of 0.78, the absorbed heating for the tungsten calorimeter will be 30 kW/cm$^2$ at the 100-MW power level. The dashed line for the tungsten calorimeter ($a$ = 0.78) agrees reasonably well with the trend found for the heat-transfer rate measurements.

The most recent theoretical calculations of the heat transfer rate distribution over the heat shield incorporate an eddy diffusivity model of the gas and a more hydrogen-rich atmosphere for Jupiter. The resulting heat transfer rates that are predicted for the heat shield are shown in Figure 24. The stagnation-point values are somewhat lower than earlier calculations presented above. The predicted heat transfer rates decrease rapidly from the stagnation-point values for both radiative and convective heating. Over the conical frustum area of the heat shield, both heat transfer rates approach constant values that are nominally 10 kW/cm$^2$. The facility capabilities are shown by the bar graphs at the right of the figure. The predicted convective heating is well matched by the facility capability for power levels between 60 and 100 MW. The predicted radiative heating at the stagnation point is about a factor of two above the facility capability. However, over the conical frustum of the heat shield, the radiative heating expected will be well matched by the facility capability. It should be noted that the conical frustum represents over 90% of the heat shield surface area.

SUMMARY

A summary of the specifications of the Giant Planet Facility is given in the table appearing in Figure 25. The arc heater was designed for the 100-MW power level so as to attain good entry heating simulation of a probe entering the atmosphere of Jupiter. The constricted-arc heater that was developed represents the most advanced state-of-the-art design in terms of the power density developed in the arc-jet flow. Such high power densities are required to obtain a test stream with significant radiative heating to the test body. The nozzle was designed for a Mach number of 1.67 so as to yield optimum radiative heating to a 4-cm diameter test body. The performance of the arc heater has been verified to the 75-MW power level. The facility power rating of 100 MW is based on the advanced design of the constrictor discs which have a potential cooling capability of 12 kW/cm$^2$ with a reasonable safety margin. Measurements of voltage, wall heat loss, and arc-heater efficiency obtained during initial development and performance tests agree well with calculated values based on theoretical modeling of the arc-heated flow. The good agreement observed allows for extrapolation to the 100-MW rating with reasonable certainty. The maximum enthalpy levels that should be attained at full power, are in excess of 400 MJ/kg and represent a reasonable simulation of the entry heating condition. The measured heat-transfer rates to an optimum 4-cm-diameter blunt test body match the expected rates to a fair degree. In particular, convective heating rates of from 11 to 18 kW/cm$^2$ generated in the facility closely approximate the expected full-scale values for a heat shield for a planetary probe into Jupiter's atmosphere. The predicted radiative heating rate of 16 kW/cm$^2$ generated in the facility at the 100-MW power level is about one third of expected full-scale values. However, the simultaneous generation of convective and radiative heat-transfer rates of these magnitudes will allow experimental studies to determine the ablation performance of such coupled convective and radiative flows. Such tests will provide heat-shield design data for use in assessing material performance and will make it possible to verify computer codes developed specifically to extrapolate material ablation performance to the severe ranges beyond the present facility limits. The degree of simulation of the entry conditions is limited by inherent constraints of the arc-heater design and performance. The high performance level achieved requires only a modest extrapolation to expected full-scale conditions.

ACKNOWLEDGMENT

The authors express their particular recognition of the contributions made by Howard A. Stine, whose analytical work forms the foundation of modern constricted-arc theory. In addition to his theoretical innovations, his active leadership in the development of electric-arc-heated facilities resulted in major advances in the technology of this field.

REFERENCES

(1) Riddell, F. R. and Winkler, H. B., "Meteorites and Re-entry of Space Vehicles at Meteor Velocities," ARS J. Vol 32, No. 70, Oct. 1962, pp. 1523-1530.

(2) Whipple, F. L., "Meteors and the Earth's Upper Atmosphere," Rev. Mod. Phys. Vol. 15, 1943, pp. 246-264.

(3) Allen, H. J., Seiff, A., and Winovich, W., Aerodynamic Heating of Conical Entry Vehicles at Speeds in Excess of Earth Parabolic Speed. NASA TR R-185, Dec. 1963.

(4) Tauber, M. E., "Atmospheric Entry into Jupiter," J. Spacecraft & Rockets. Vol. 6, No. 10, Oct. 1969, pp. 1103-1109.

(5) Nicolet, W. E., Howe, J. T., and Mezines, S. A., Outer Planet Probe Entry Thermal Protection: Part II: Heat-Shielding Requirements, AIAA Paper

No. 74-701, AIAA/ASME Thermophysics and Heat Transfer Conference, Boston, Massachusetts, July 1974.

(6) Moss, J. N., Anderson, E. C., and Bolz, C. W., Jr., "Viscous-Shock Layer Solution with Radiation and Ablation Injection for Jovian Entry," Paper 75-671. AIAA 10th Thermophysics Conference, Denver, Colorado, May 1975.

(7) Nelson, H. F. and Mezines, S. A., "Parametric Analysis of Jupiter Probe Heat Shield Recession Uncertainties," AIAA Paper 78-919. Second AIAA/ASME Thermophysics and Heat Transfer Conference, Palo Alto, California, May 1978.

(8) Davy, W. C., Menees, G. P., Lundell, J. H., and Dickey, R. R., "Carbonaceous Materials Subjected to Extreme Heating," AIAA Paper 78-866. Second AIAA/ASME Thermophysics and Heat Transfer Conference, Palo Alto, California, May 1978.

(9) Moss, J. N., Anderson, E. C., and Bolz, C. W., Jr., "Aerothermal Environment for Jovian Entry Probes," AIAA Progress in Astronautics and Aeronautics-Thermophysics of Spacecraft and Outer Planet Entry Probes, Vol. 56, A. M. Smith, Ed., New York, pp. 333-354, 1977.

(10) Hunter, D. M., "Atmospheres and Ionospheres," Jupiter. T. Gehrels, Ed., University of Arizona Press, Tucson, Arizona, 1976.

(11) Atreta, S. K., "The Atmosphere of Jupiter," Outer Planetary Probe Mass Spectrometer Study. NASA CR 137886, June 1976.

(12) The Planet Jupiter (1970). NASA SP-8069, Dec. 1971.

(13) Howe, J. J. and Viegas, J. R., Solutions of the Ionized Radiating Shock Layer Including Reabsorption and Foreign Species Effects and Stagnation Region Heat Transfer. NASA TR R-159, 1963.

(14) Yoshikawa, K. K., Analysis of Radiative Heat Transfer for Large Objects at Meteoric Speeds. NASA TN-D-4051, 1967.

(15) Moss, J. W., Jones, J. J., and Simmonds, A. L., "Radiative Penetration through a Blown Shock Layer for Jupiter Entry Conditions," AIAA Paper 78-908. Second AIAA/ASME Thermophysics and Heat Transfer Conference, Palo Alto, California, May 1978.

(16) Beachler, J. C., Operating Characteristics of the Air Force Flight Dynamics Laboratory Reentry Nose Tip (RENT) Facility. National Bureau of Standards Special Publication 336, Paper No. 55, 1970.

(17) Drell, I. L. and Belles, F. E., Survey of Hydrogen Combustion Properties. NACA Report 1383, 1957.

(18) Zabetakis, M. G., Research on the Combustion and Explosion Hazards of Hydrogen-Water Vapor-Air Mixtures. U. S. Atomic Energy Commission Report AECU-3327, Sept. 1956.

(19) Stine, H. A. and Watson, V. R., The Theoretical Enthalpy Distribution of Air in Steady Flow Along the Axis of a Direct-Current Electric Arc. NASA TN D-1331, 1962.

(20) Stine, H. A., Watson, V. R., and Shepard, C. E., Effect of Axial Flow on the Behavior of the Wall-Constricted Arc. AGARDOGRAPH-84, Part 1—Arc Heaters and MHD Accelerators for Aerodynamic Purposes, 1964, pp. 451-485.

(21) Shepard, C. E., Ketner, D. M., and Vorreiter, J. W., A High Enthalpy Plasma Generator for Entry Heating Simulation. NASA TN D-4588, 1968.

(22) Winovich, W., On the Equilibrium Sonic-Flow Method for Evaluation Electric-Arc Air-Heater Performance. NASA TN D-2132, 1964.

(23) Clark, K. J., Nelson, E. V., Nicolet, W. E., Carlson, D. L., Balakrishnan, A., and Reese, J. J., Jr., A Study of the Feasibility of Investigating Radiation/Turbulent-Mixing-Layer Interactions in a Constricted Arc. Aerotherm Final Report 75-167, NASA Contract NAS1-13666, Oct. 1975.

(24) Maecker, H. and Steinberger, S., "Further Development of the Cascade Arc Constrictor for High Power," Zeitschrift für Angewandte Physik. Vol. 33, 1957, pp. 456.

(25) Cobine, J. D., Gaseous Conductors. Dover Pub., Inc., New York, 1958.

(26) Winovich, W. and Carlson, W. C. A., The 60-MW Shuttle Interaction Heating Facility. 25th International Instrumentation Symposium, Anaheim, California, May 1979.

(27) Winovich, W., "Total Radiation at the Stagnation Point of Blunt Bodies at Stagnation Temperatures to 15000 K," AIAA Paper 68-405. AIAA 3rd Aerodynamic Testing Conference, San Francisco, California, April 1968.

(28) Winovich, W. and Croce, P. A., "Spectroscopic Study of the Gas-Cap Radiation Intensity for Simulated Martian Atmospheric Probes," J. Quant. Spectrosc. Radiat. Transfer. Vol. 8, Pergamon Press, 1968, pp. 171-190.

(29) Czysz, P., Correlation of Wind Tunnel Blockage Tests. Wright-Patterson AFB, Report No. ASD-TDR-63-230, April 1963.

(30) Green, M. J. and Nicolet, W. E., "Aerothermodynamic Environment for Jovian Entry with a Silica Heat Shield," AIAA Paper 78-186. AIAA 16th Aerospace Sciences Meeting, Huntsville, Alabama, Jan. 1978.

(31) Fay, J. A. and Riddell, F. R., "Theory of Stagnation Point Heat Transfer in Dissociated Air," J. of Aeronautical Sciences. Vol. 25, No. 2, 1958.

(32) Marvin, J. G. and Deiwert, G. S., Convective Heat Transfer in Planetary Gases. NASA TR R-224, July 1965.

(33) Hiester, N. K. and Clark, C. F., Relative Operating Capabilities of Selected Electric-Arc Reentry Environment Simulators," Stanford Research Institute Report No. 4, Tech. Rept. No. 1 (SRI Project No. PMU-4512), May 1964.

(34) Shepard, C. E., Vorreiter, J. W., Stine, H. A., and Winovich, W., A Study of Artificial Meteors as Ablators. NASA TN D-3740, Mar. 1967.

(35) Vinokur, M., Inviscid Hypersonic Flow Around Blunt Bodies. LMSD, Tech Note LMSD-48454, Mar. 1959.

(36) Eckert, E. R. G., Introduction to the Transfer of Heat and Mass. McGraw-Hill Book Company, Inc., New York, 1950.

(37) Kauzmann, W., "Physical Chemistry Monograph Series. Thermal Properties of Matter," Vol. I, Kinetic Theory of Gases. W. A. Benjamin, Inc., New York, 1966.

(38) Baines, D. J., A Comparative Theoretical Evaluation of Five Commonly Used Types of Heat Flux Sensor." Report HSA 27, Dept. of Supply, Australian Defense Scientific Service Weapons Research, 1970.

(39) Kirchhoff, R. H., Calorimetric Heating-Rate Probe for Maximum-Response-Time Interval. NASA TM X-54,019, Jan. 1964.

(40) Touloukian, Y. S., Ed. Thermophysical Properties of High Temperature Solid Materials, Vol. I: Elements. The Macmillan Company, New York, 1966.

## APPENDIX A

## VARIATION OF RADIATIVE HEATING WITH MACH NUMBER

The radiative heat-transfer rate to the blunt body is given by the optically-thin expression:

$$\dot{q}_r = 2a(\rho\kappa)\delta\sigma T^4 \qquad (1\text{-A})$$

For this formulation, the flow conditions are related to the state of the gas that exists just behind the normal shock. The effective mass-absorption coefficient for a radiating hydrogen-helium plasma is obtained from the detailed gas-cap calculations given in Ref. 30. An empirical fit to the results is given by:

$$(\rho\kappa) = 1.208 \times 10^{-9}\, p^{0.882}\, \delta^{-0.451}\, T^{5.625},\ \text{cm}^{-1} \qquad (2\text{-A})$$

This empirical fit to the detailed calculations applies for shock-layer thicknesses from 1 to 3 cm and for temperatures from 14000 to 17000 K. The conditions correspond to the state just behind the normal shock. By combining Equations (1-A) and (2-A), one obtains the heat transfer to the test body in terms of the local facility conditions in the gas-cap region:

$$\dot{q}_r = 1.369 \times 10^{-23} a\, \delta^{0.549}\, p^{0.882}\, T^{5.625},\ \text{kW/cm}^2 \qquad (3\text{-A})$$

The surface absorptivity is taken as the Planck mean value:

$$a = \frac{\int_0^\infty a(\lambda)/\lambda^5 (e^{HC/k\lambda T} - 1)\, d\lambda}{\int_0^\infty 1/\lambda^5 (e^{HC/k\lambda T} - 1)\, d\lambda} \qquad (4\text{-A})$$

For a tungsten surface, the spectral absorptivity of the material is given in Ref. 40. For the range of interest, the Planck-mean absorptivity can be evaluated for a temperature of 14000 K and taken as constant. Then, for tungsten in a hydrogen-helium plasma, a = 0.78; for a graphite surface, a = 1.0. Consequently, when the flow conditions are specified, the radiative heating is only a function of the shock standoff distance $\delta$ and the Mach number of the stream which determines the state behind the normal shock.

The Mach number for the facility is selected such that the highest radiative flux is obtained from the gas-cap region of a test body. This design concept defines an optimum test-body size that is the largest blunt body that will maintain supersonic flow. The optimum test body, therefore, is defined in terms of a maximum allowable blockage ratio for the supersonic free-jet stream. Studies show that the blockage ratio for maintaining supersonic flow varies with the Mach number; larger blockage ratios can be employed for higher Mach numbers. For supersonic free jets, the maximum blockage ratio criterion for a blunt test body shape is given by:

$$BR = 0.176\sqrt{M^2 - 1} \qquad (5\text{-A})$$

For Mach numbers greater than 3, the blockage ratio must be taken as 0.5. It follows, therefore, that the test body size—as well as the local stagnation flow conditions—is uniquely determined by the Mach number selected for the facility. When the test-body size is established by the blockage criterion given above, the shock standoff distance must be calculated in order to find the radiative flux. Shock standoff distance for the blunt body shape is obtained from the analysis for blunt ellipsoids of Ref. 35. A correlation of the solution for an ellipsoid with a bluntness ratio of 0.25—which closely approximates the test body shape—gives the shock standoff distance as:

$$\delta/r_b = 0.583/\sqrt{\rho_2/\rho_1 - 1} \qquad (6\text{-A})$$

The parametric study has been performed for an assumed total state corresponding to facility operations near the rated limit (100 MW). For this study, the stagnation state for the arc heater was chosen as a total pressure of 5 atm and a stagnation enthalpy of 500 MJ/kg. The procedure for the parametric study is as follows: (1) select a value for the free-stream Mach number; (2) calculate the area ratio and find the exit diameter of the nozzle (assuming a throat diameter of 6 cm); (3) determine the gas-cap conditions $\rho_2/\rho_1$, $p_2$, and $T_2$ for normal shock flow; (4) use the blockage criterion given by Equation (5-A) to determine the test-body size; (5) calculate the shock standoff distance for the blunt shape using Equation (6-A); and (6) calculate the radiative heat-transfer rate to the test body using Equation (3-A). For the calculations, the properties for the nozzle flow have been obtained from isentropic flow relations and normal shock equations for a perfect gas. An effective isentropic coefficient of 1.23 has been assumed.

## APPENDIX B

### HEAT LOSS FORMULATIONS FOR THE CONSTRICTED ARC

The efficiency of the constricted-arc heater is determined by the geometry and the magnitudes of the convective and radiative losses from the arc column. These losses are expressed in nondimensional form in the equation defining the conversion efficiency of the heater:

$$\eta = 1/[1 + 4(L/D)C_H F] \qquad (1\text{-B})$$

where the radiation component is given in terms of the factor:

$$F = 1 + \dot{q}_r/\dot{q}_c$$

The convective losses are determined by the Stanton number. At low enthalpy levels, the arc-column radiation is negligible and convection losses, only, determine the arc-heater efficiency. As the enthalpy level increases, the arc-column temperature increases and the radiative losses from the arc core become important. At very high temperatures (i.e., 15,000 K), the radiation from the arc core becomes the dominant loss mechanism. The variation in the efficiency changes, then, as the relative importance of the radiative loss increases. The convective and radiative losses can be treated separately as suggested by the form of the efficiency relation.

#### Convective Loss

The Stanton number for flow within tubes is obtained from the turbulent pipe-flow relation as (36):

$$C_H = 0.0276/(N_r)^{0.2} \qquad (2\text{-B})$$

where a Prandtl number of 0.74 has been assumed. The Reynolds number for the constrictor tube flow is found by using the equilibrium sonic flow relation. This relation applies strictly for the sonic region at the end of the constrictor; however, to first order, the result can be applied to the entire constrictor length. This application is supported by the observation that the heating remains virtually constant all along the constrictor tube (e.g., Figure 17). The mass flux in the constrictor tube, then, is given by:

$$\rho V = 15.3\, p_t/\sqrt{\bar{h}_t}\,,\ \text{g/sec-cm}^2 \qquad (3\text{-B})$$

The viscosity for the hydrogen-helium gas mixture is obtained by using the scaling relation for the hard-sphere theory (37). That is,

$$\mu = (5/16\sqrt{\pi})(mR_gT)^{\frac{1}{2}+2/n}/N_o\xi^2 \qquad (4\text{-B})$$

The factor $n$ accounts for gas interaction effects; for the hydrogen-helium mixture, the value $n = 12$ has been assumed (37). The collision cross section for the mixture is taken as the root-mean-square value of each component. By applying this relation to the viscosity data for either pure hydrogen or pure helium, the viscosity of the mixture is obtained as $\mu_o = 1.4 \times 10^{-4}$ poise ($T_o = 273$ K). The variation of viscosity with temperature is obtained from the same relation as

$$\mu = 3.5 \times 10^{-4}(T/1000)^{0.70},\ \text{poise} \qquad (5\text{-B})$$

The Reynolds number for the constrictor tube can be expressed in terms of the facility operating parameters by combining Equations (3-B) and (5-B) and taking the constrictor diameter as 6 cm. The result is:

$$N_r = 2.87 \times 10^{-5}\, p_t/\sqrt{\bar{h}_t}\,(T/1000)^{0.70} \qquad (6\text{-B})$$

Note that for the range of interest for the Giant Planet Facility ($p_t = 5$ atm and $h_t \leq 600$ MJ/kg) the Reynolds number is of the order of $10^5$, or greater. Accordingly, for flow within tubes, the Reynolds number is in the range for turbulent flow ($N_r > 2000$); and the use of Equation (2-B) is justified. By using the relations given above, the convective heat-transfer rate to the constrictor wall is expressed in terms of the operating conditions as:

$$\dot{q}_{c,w} = 15.3\, C_H\, p_t\sqrt{\bar{h}_t},\ \text{kW/cm}^2 \qquad (7\text{-B})$$

Constrictor wall heating is tabulated below for the operating range of interest.

#### Radiative Loss

The radiative loss from the arc heater is obtained by adopting a simple radiation model in which the arc filament is represented by a constant-temperature core with an effective diameter equal to half the diameter of the constrictor. This model is suggested by results from the ARCFLO computer program for the constricted arc which gave stream profiles. The uniform core temperature is taken as the centerline value. For the operating range of interest for the Giant Planet Facility, the ratio of the centerline temperature to the temperature corresponding to the mass-average (measured) enthalpy is taken as

$$T_o/\bar{T}_t = 1.43$$

This value, predicted from the ARCFLO computer solutions, is in good agreement with spectroscopic measurements made at the test section which gave a value of 1.35. Radiant heating to the wall is found from the one-dimensional, constant temperature solution for an optically-thin slab given above (Equation (3-A)). The appropriate value for the thickness is D/4, the centerline temperature ratio is 1.43, and the surface absorptivity of the wall is taken as unity. For this radiating filament model of the arc, the heating to the walls becomes:

$$\dot{q}_{r,w} = 4.785 \times 10^{-23} D^{0.549}\, p_t^{\,0.882}\, \bar{T}_t^{\,5.625}\,,\ \text{kW/cm}^2 \qquad (8\text{-B})$$

The radiation factor $F$ is obtained from Equations (1-B), (7-B), and (8-B). Note that the radiation factor is a weak function of pressure, and calculated results for the nominal operating pressure of 5 atm are valid over wide pressure limits.

The table below gives the results from a heat loss and efficiency analysis for the 6-cm constrictor with a hydrogen-helium gas mixture. The equation of state for this calculation was obtained from the ARCFLO computer program for hydrogen-helium gas.

Effect of Arc-Column Radiation on the Conversion Efficiency; $p_t$ = 5 atm

| | | | | | | | | |
|---|---|---|---|---|---|---|---|---|
| $\bar{h}_t$, MJ/kg | 100 | 150 | 200 | 250 | 300 | 350 | 400 | 500 |
| $\bar{T}_t$, °K | 4000 | 4700 | 7400 | 10200 | 11900 | 13000 | 14000 | 15000 |
| $N_r$ | 36480 | 27480 | 18960 | 14450 | 12210 | 10820 | 9750 | 8425 |
| $C_H$ | 0.00338 | 0.00357 | 0.00384 | 0.00406 | 0.00420 | 0.00431 | 0.00440 | 0.00452 |
| $\dot{q}_{c,w}$, kW/cm$^2$ | 2.59 | 3.34 | 4.15 | 4.91 | 5.56 | 6.17 | 6.73 | 7.73 |
| $\dot{q}_{r,w}$, kW/cm$^2$ | 0.10 | 0.24 | 3.14 | 14.18 | 45.44 | 74.84 | 113.53 | 166.98 |
| F | 1.038 | 1.073 | 1.755 | 3.887 | 9.166 | 13.133 | 17.865 | 22.596 |
| $\eta(\dot{q}_r = 0)$ | 0.476 | 0.462 | 0.443 | 0.430 | 0.422 | 0.416 | 0.410 | 0.404 |
| $\eta$(exact) | 0.466 | 0.444 | 0.312 | 0.134 | 0.074 | 0.051 | 0.038 | 0.030 |

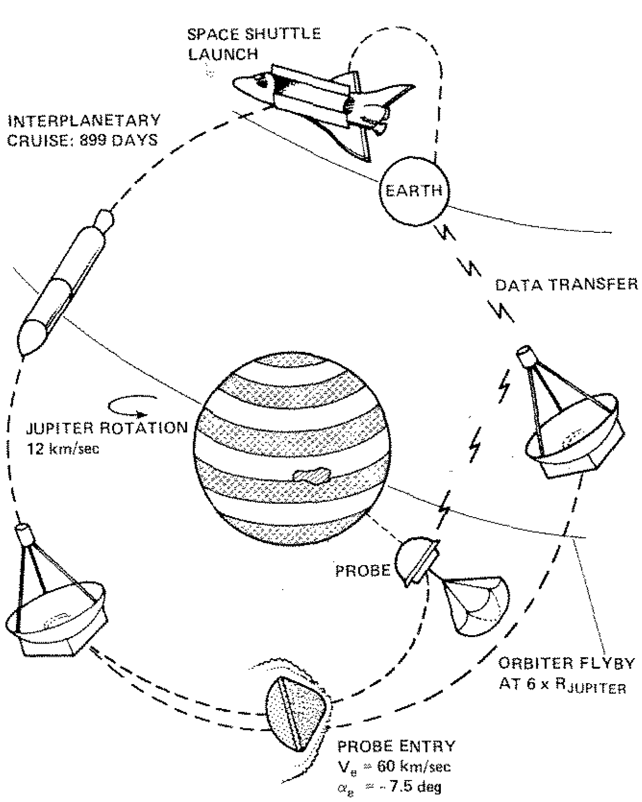


Figure 1 - Planetary Mission to Investigate the Atmosphere of Jupiter with an Unmanned Space Probe.

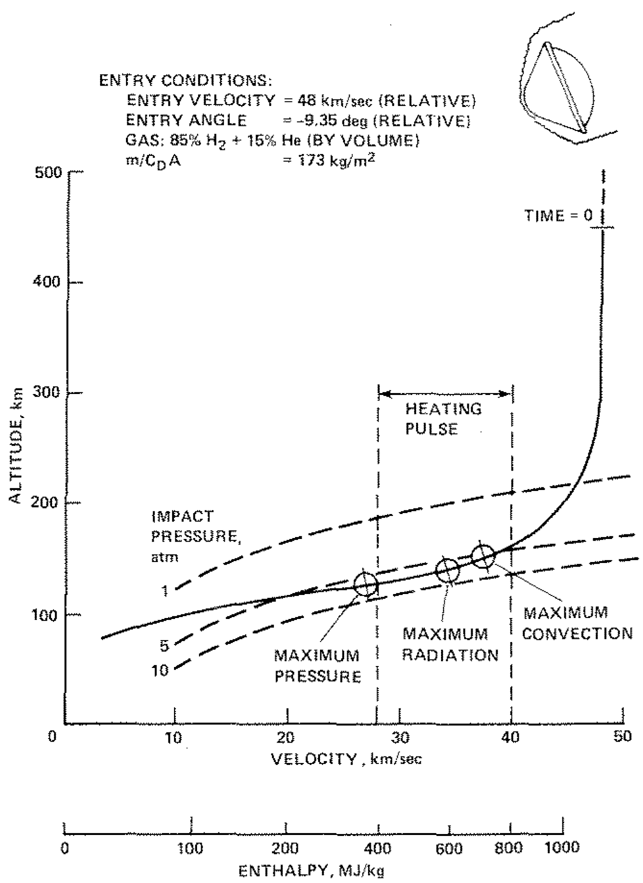


Figure 2 - Jupiter Entry Trajectory for a Planetary Probe.

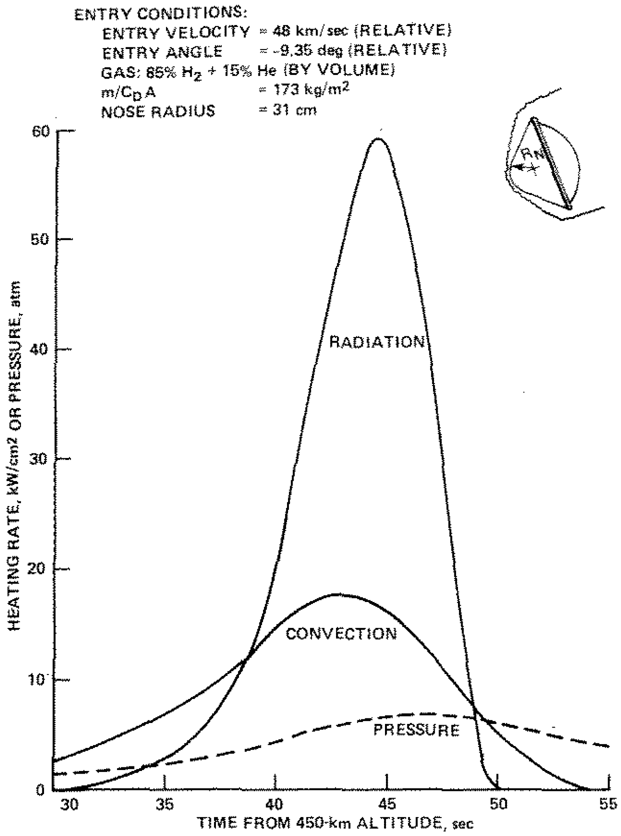


Figure 3 - Stagnation-Point Heat-Transfer Rates and Pressure for the Entry Probe.

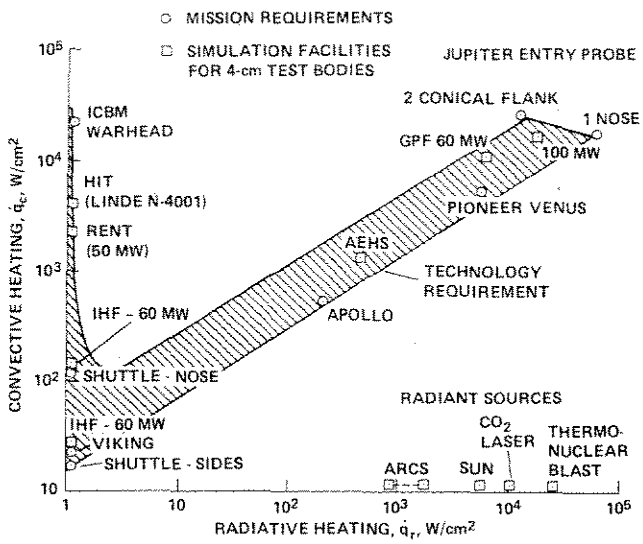


Figure 4 - Technology Requirements for Simulation of Entry Heating for Various Missions.

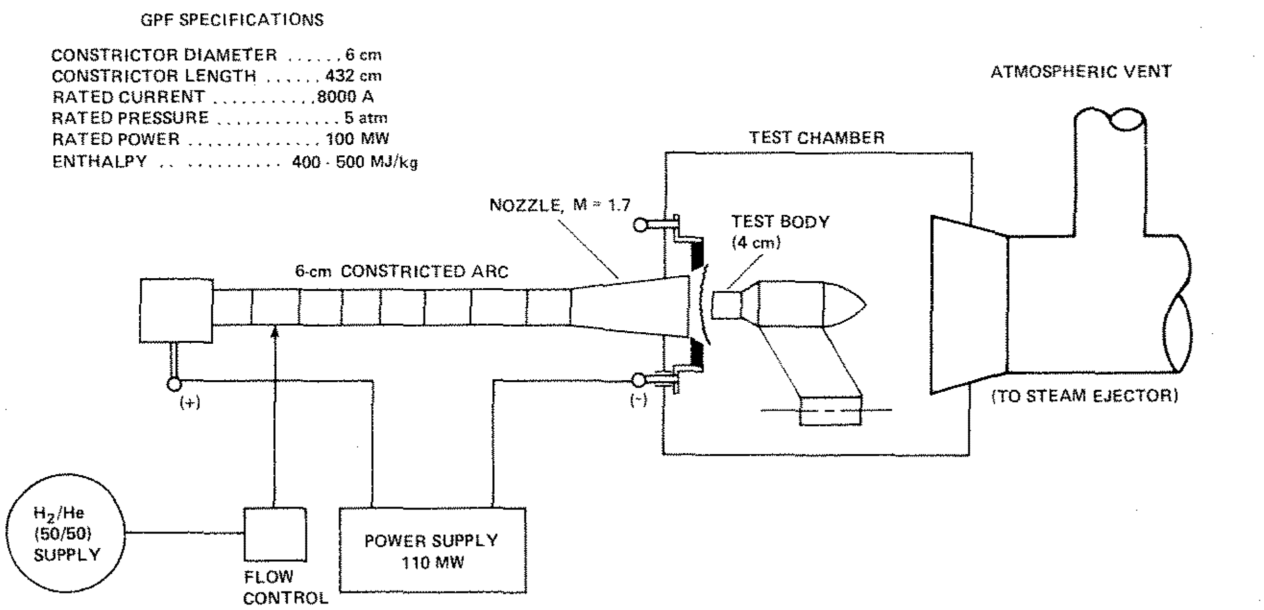


Figure 5 - Giant Planet Facility—Schematic View.

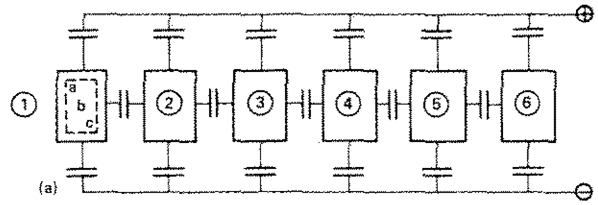


a - Rectifier Module Switching Arrangement.

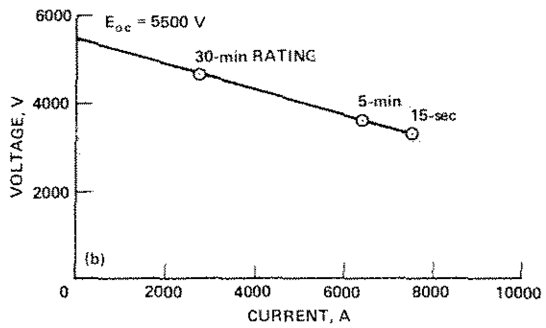


b - Voltage-Current Characteristic of a Single Rectifier Module.

| POWER SUPPLY CONFIGURATION | | | DUTY CYCLE | | | | | | | | |
|---|---|---|---|---|---|---|---|---|---|---|---|
| | | | 30 min ON | | | 5 min ON | | | 15 sec ON | | |
| NO. IN SERIES | NO. IN PARALLEL | $E_{oc}$ V | $E_R$ V | $I_R$ A | $P_R$ MW | $E_R$ V | $I_R$ A | $P_R$ MW | $E_R$ V | $I_R$ A | $P_R$ MW |
| 6 | 1 | 33000 | 28050 | 2700 | 76 | 21600 | 6400 | 138 | 19800 | 7500 | 148 |
| 3 | 2 | 16500 | 14025 | 5400 | 76 | 10800 | 12800 | 138 | 9900 | 15000 | 148 |
| 2 | 3 | 11000 | 9350 | 8100 | 76 | 7800 | 16200 | 126 | 7800 | 16200 | 126 |
| 1 | 6 | 5500 | 4675 | 16200 | 76 | 4675 | 16200 | 76 | 4675 | 16200 | 76 |

c - Power Supply Rating for Various Configurations and Duty Cycles.

Figure 6 - Direct-Current Power Supply for Electric Arc Heaters.

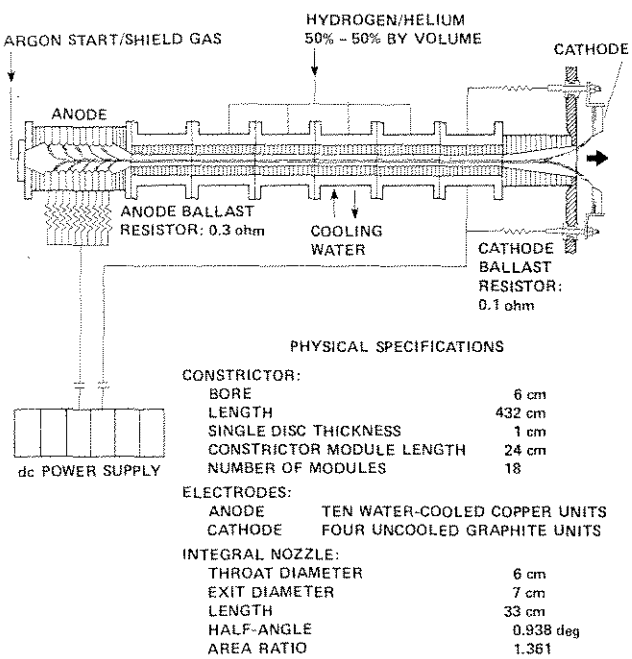


Figure 7 - The 6-cm Constricted-Arc Heater for Operation with Hydrogen-Helium Gas Mixtures.

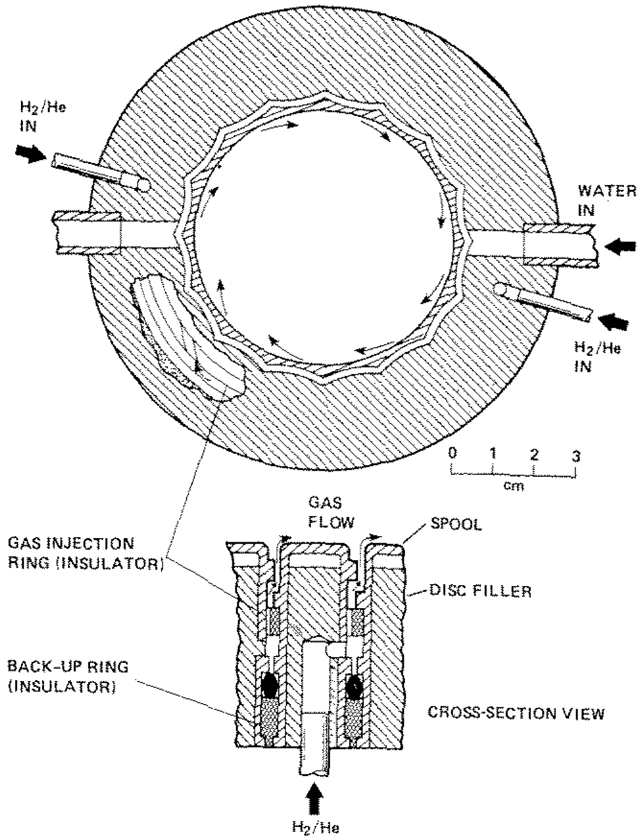


Figure 8 - Water-Cooled Constrictor Disc Design.

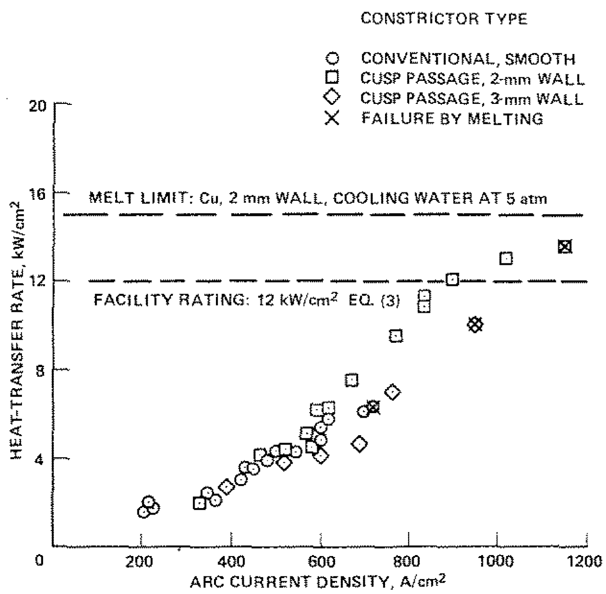


Figure 9 - Cooling Capabilities of Constrictor Disc Designs.

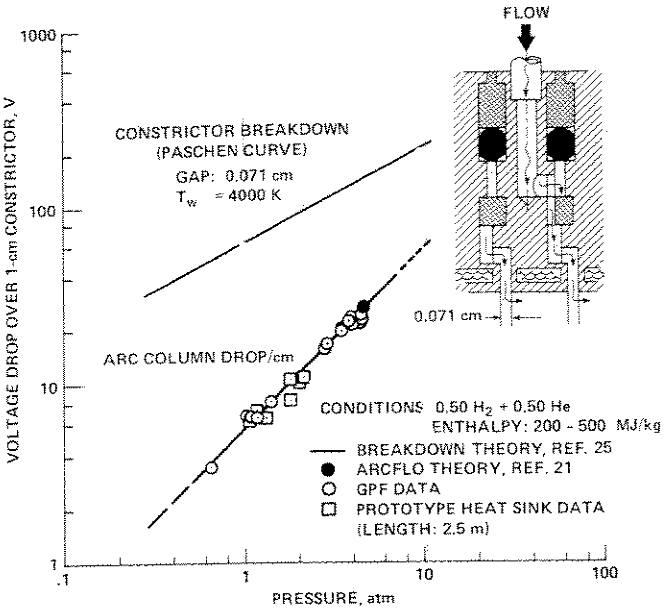


Figure 10 - Voltage Developed over the 1-cm Thick Constrictor Disc in the 6-cm Constricted-Arc Heater of the Giant Planet Facility.

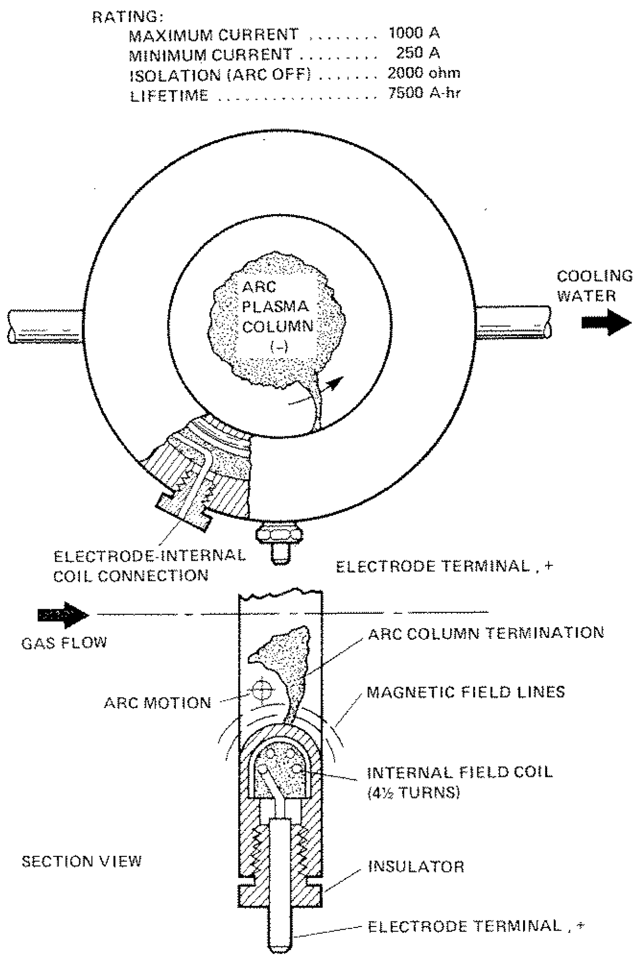


Figure 11 - Water-Cooled Copper Anode Design.

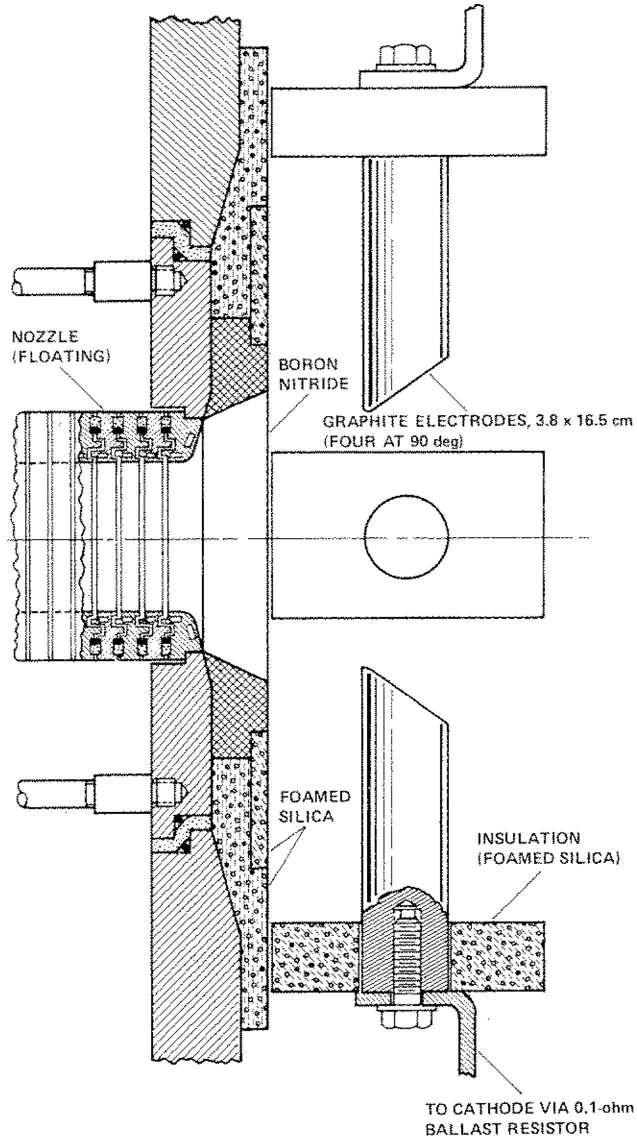


Figure 12 - Cathode Design for Giant Planet Facility Arc Heater.

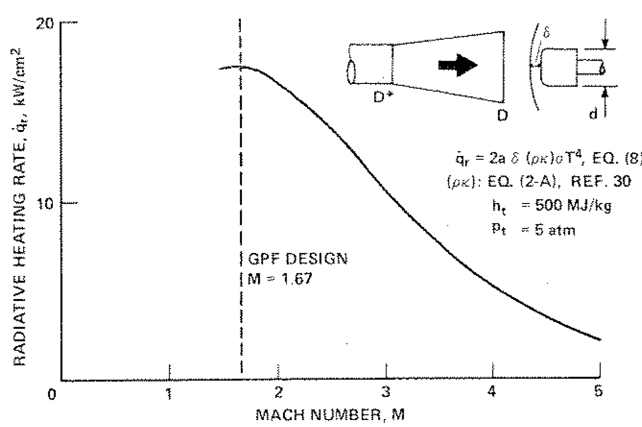


Figure 13 - Effect of the Facility Mach Number on Radiative Heating to an Optimum Test Body.

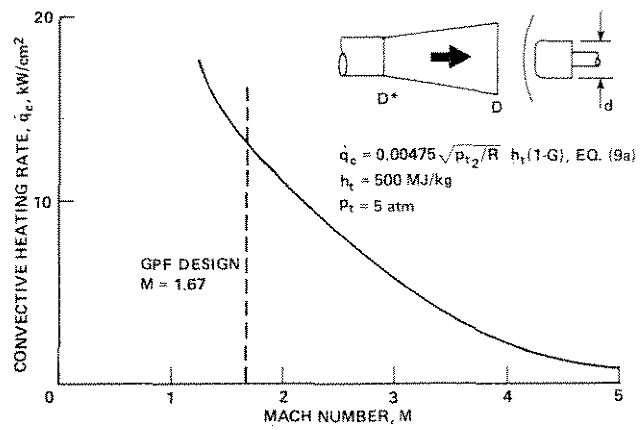


Figure 14 - Effect of the Facility Mach Number on Convective Heating to an Optimum Test Body.

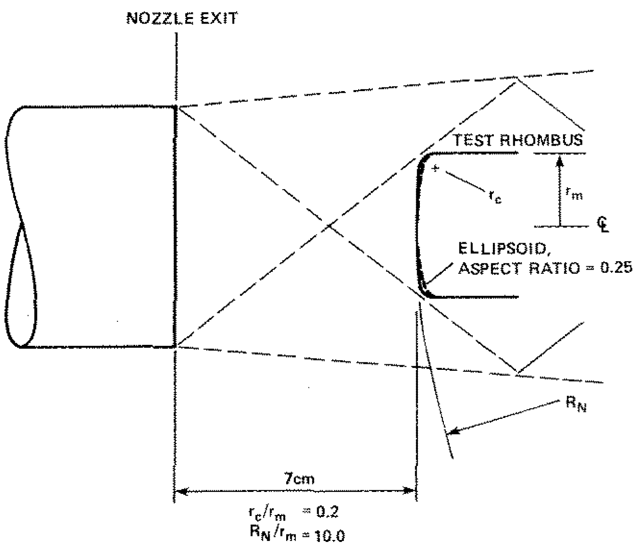


| TEST BODY SIZE, $r_m$, cm | NOZZLE BLOCKAGE RATIO, EQ. 10 |
|---|---|
| 2.06 | 35% (DESIGN VALUE) |
| 1.27 | 13% |
| 2.50 | 51% |

Figure 15 - Optimum Test Body Geometry for the Giant Planet Facility.

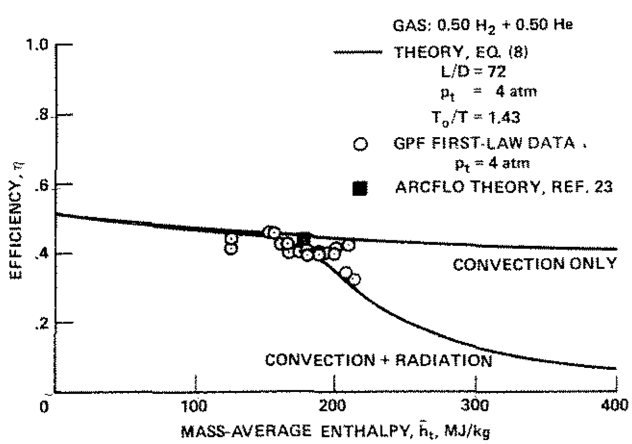


Figure 16 - Efficiency of the 6-cm Constrictor Arc Heater for a Hydrogen-Helium Gas Mixture.

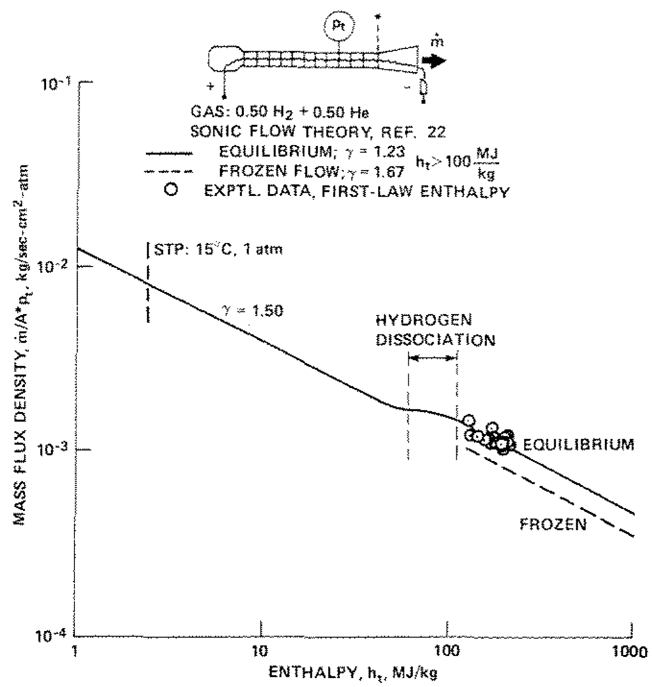


Figure 17 - Sonic Flow Measurements for the 6-cm Diameter Constricted-Arc Heater of the Giant Planet Facility.

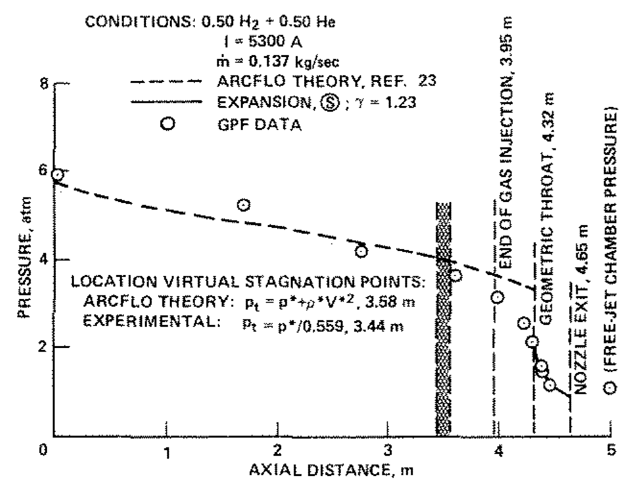


Figure 18 - Pressure Distribution along the Bore in the 6-cm Constricted-Arc Heater.

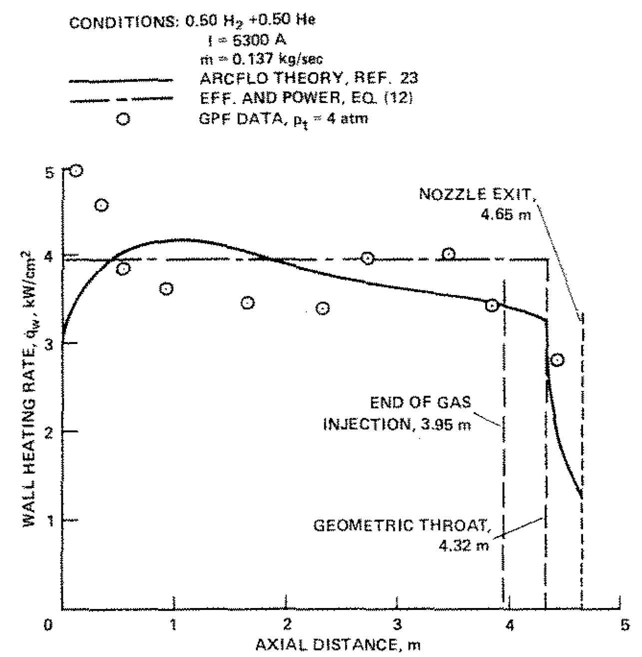


Figure 19 - Constrictor Disc Wall Heat-Transfer Rate for the 6-cm Constricted-Arc Heater.

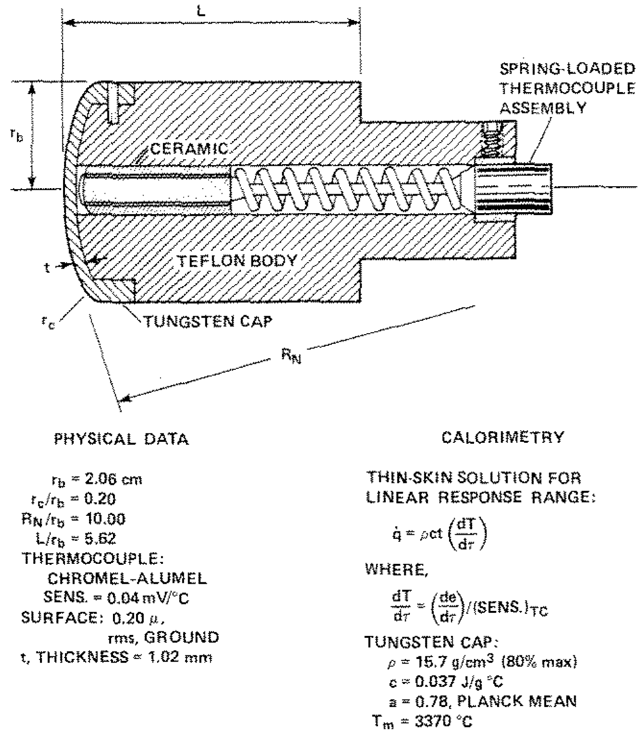


Figure 21 - Thin-Skin, Transient, Expendable Calorimeter Design.

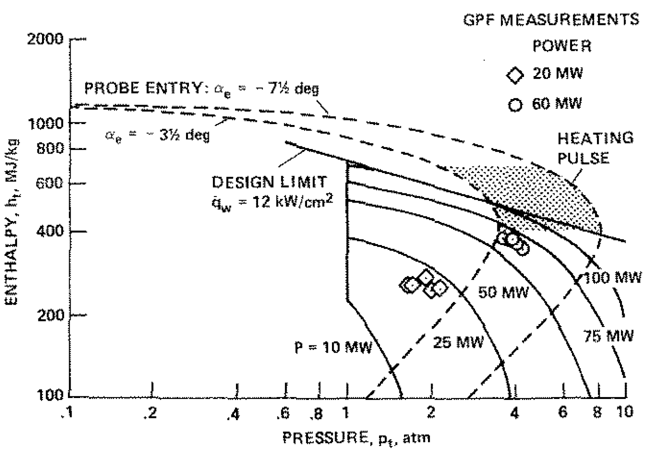


Figure 20 - Operating Envelope of the 6-cm Constricted-Arc Heater with a 50% Hydrogen-50% Helium Gas Mixture.

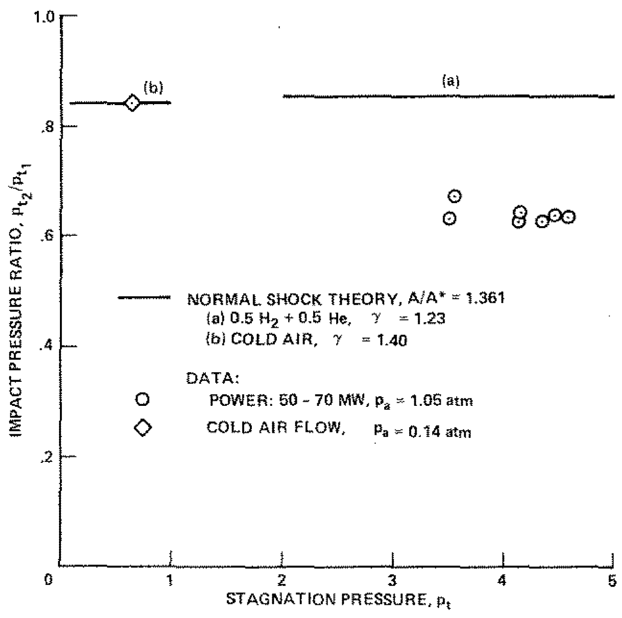


Figure 22 - Impact Pressure Ratio for a 4-cm Diameter Test Body.

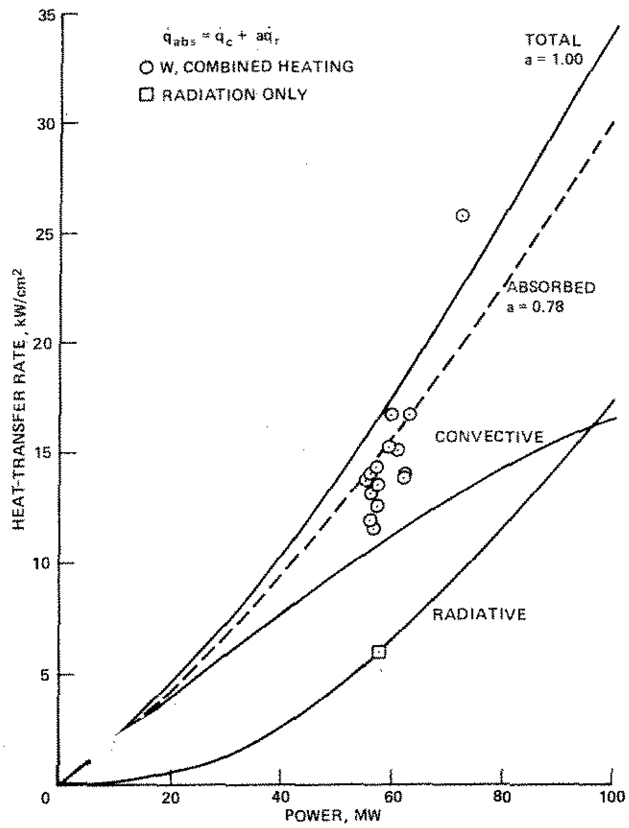


Figure 23 - Heat-Transfer Rate to the 4-cm Diameter Blunt Test Body.

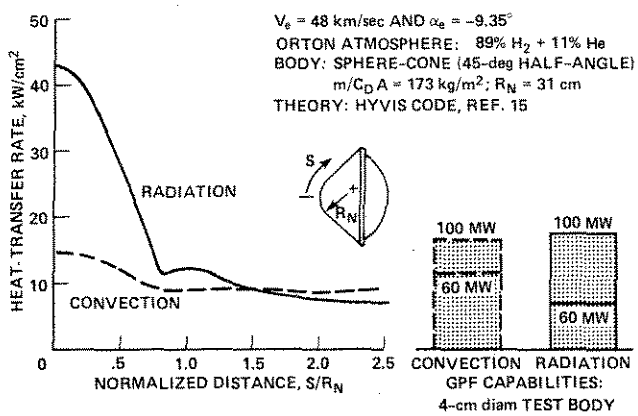


Figure 24 - Heat-Transfer Rate Distribution over the Jupiter Probe Heat Shield at Peak Heating.

PHYSICAL SPECIFICATIONS

| | |
|---|---|
| ARC HEATER | |
| WORKING FLUID | 50% $H_2$ AND 50% He, BY VOLUME |
| CONSTRICTOR DIAMETER | 6.0 cm |
| CONSTRICTOR LENGTH | 432.0 cm |
| UPSTREAM ELECTRODE LENGTH | 45.7 cm |
| OVERALL ARC LENGTH (ELECTRODE CTR.-CTR. DISTANCE) | 489.7 cm |
| UPSTREAM ELECTRODE | EIGHT COPPER ELECTRODES, MAGNETIC SPIN |
| DOWNSTREAM ELECTRODE | FOUR GRAPHITE ELECTRODES BEYOND EXIT |
| NOZZLE | |
| THROAT DIAMETER | 6.0 cm |
| EXIT DIAMETER | 7.0 cm |
| AREA RATIO | 1.361 |
| DESIGN MACH NUMBER (ISENTROPIC COEFF. = 1.23) | 1.67 |
| THROAT LOCATION | 432.0 cm (STATION) |
| EXIT LOCATION | 465.0 cm (STATION) |
| NOZZLE EXPANSION HALF-ANGLE | 0.938 deg |

PERFORMANCE SPECIFICATIONS

| ARC HEATER | | ATTAINED | RATED |
|---|---|---|---|
| CURRENT | A | 6100 | 7800 |
| FLOW RATE | kg/sec | 0.160 | 0.160 |
| VOLTAGE | V | 11790 | 12800 |
| POWER | MW | 71.9 | 100 |
| PRESSURE @ STA. 344 cm | atm | 4.94 | 5 |
| EFFICIENCY | percent | 35.9 | 33.3 |
| ENTHALPY (CENTERLINE) | MJ/kg | 311 | 410 |
| CONSTRICTOR WALL HEATING | kW/cm² | 6.2 | 12 |
| TEST BODY | | | |
| STAGNATION HEATING (TOTAL) | kW/cm² | 25.8 | 34.0 |
| CONVECTIVE | kW/cm² | 16.3 | 17.5 |
| RADIATIVE | kW/cm² | 9.5 | 16.5 |
| STAGNATION PRESSURE | atm | 2.71 | 3.10 |
| FREE-JET CHAMBER PRESSURE | atm | 1.05 | 1.05 |
| TEST BODY LOCATION | cm | 7.0 | 7.0 |

NOTES:

(1) CONSTRICTOR HEATING MEASURED AT STA. 52 cm, A MAXIMUM HEATING LOCATION
(2) RATED POWER CORRESPONDS TO CONSTRICTOR HEATING LIMIT OF 12 kW/cm²
(3) EFFICIENCY FOR RATED CONDITION CALCULATED FROM EQ. (12), FIG. 16

Figure 25 - Summary of Giant Planet Facility Specifications.